# Studies on Gelator Molecule for the Fabrication of Alkali Metal Ion-based Gels and Drug Delivery

M.Sc. Thesis

By

# **ARDRA T M**



# DEPARTMENT OF CHEMISTRY INDIAN INSTITUTE OF TECHNOLOGY INDORE MAY, 2025

# Studies on Gelator Molecule for the Fabrication of Alkali Metal Ion-based Gels and Drug Delivery

# **A THESIS**

Submitted in partial fulfilment of the requirements for the award of the degree

of

**Master of Science** 

by

**ARDRA T M** 



# DEPARTMENT OF CHEMISTRY INDIAN INSTITUTE OF TECHNOLOGY INDORE MAY, 2025



# INDIAN INSTITUTE OF TECHNOLOGY INDORE

# **CANDIDATE'S DECLARATION**

I hereby certify that the work being presented in the thesis entitled "Studies on Gelator Molecule for the Fabrication of Alkali Metal Ion-based Gels and Drug Delivery" in the partial fulfillment of the requirements for the award of the degree of MASTER OF SCIENCE and submitted to the Department of Chemistry, Indian Institute of Technology Indore, is an authentic record of my work carried out during the period from July 2024 to May 2025 under the supervision of Dr. Suman Mukhopadhyay, Professor, IIT Indore.

The matter presented in this thesis has not been submitted by me for the award of any other degree of this or any other institute.

0 ..

Ardra T M

This is to certify that the above statement made by the candidate is correct to the best of my knowledge.

Prof. Suman Mukhopadhyay

# ACKNOWLEDGEMENTS

I am deeply grateful to God for blessing me with the opportunity, strength, and guidance throughout this journey. I also want to express my sincere appreciation to everyone who has supported me in completing this project successfully.

First and foremost, I would like to extend my heartfelt thanks to my supervisor, Prof. Suman Mukhopadhyay, for his continuous guidance and unwavering support throughout the duration of my work. It has been an honor to work under his mentorship.

I am also sincerely grateful to my mentor, Ms. Ritika Munjal, for her invaluable guidance and assistance at every stage of this project. My thanks go to my lab members as well for their constant encouragement and support.

I am also greatly thankful to Hiba K P and Safwana Shirin K M for their companionship over the whole 2 years and the support they provided.

Finally, I would like to express my deepest appreciation to my parents, family, and friends, whose unending support and encouragement have been a constant source of strength.

Thanks to the generosity and guidance of these amazing individuals, I have made significant progress in this project. Without their help, I would not have been able to achieve the milestones I have reached in this research.

#### ARDRA T M

Department of Chemistry, IIT Indo

# DEDICATION TO MY PARENTS AND BROTHER

# **ABSTRACT**

A novel low molecular weight gelator molecule G10 (5-(((1H-imidazol-2-yl) methylene)amino)isophthalic acid)) (MW-259) was synthesised from readily available materials in a single-step process. This molecule was characterized using various spectroscopic techniques, and the interaction between the molecules that aid in forming the gel was analyzed using FTIR and PXRD techniques. The organogel fabricated from this molecule exhibited stimulus responses towards metal ions and fluoride ions. Metallogels of this molecule with alkali metal ions were also fabricated. The rheological and thixotropic properties of the gels were also assessed. Additionally, G10-Dox organogel was fabricated from this molecule, which has injectable and self-healing properties for the delivery of the drug doxorubicin.

# TABLE OF CONTENTS

LIST OF FIGURES	viii
LIST TABLES	xi
LIST OF SCHEMES	xii
NOMENCLATURE	xiii
ACRONYMS	xiv
CHAPTER 1: Introduction	1-6
1.1 General Introduction	1-2
1.2 Classification of gels	2-3
1.3 Synthesis and fabrication of gels	3
1.4 Properties and characterizations of gels	4-5
1.5 Drug delivery	5-6
CHAPTER 2: Literature survey	7-9
2.1 Literature and motivation	7-9
2.2 Objectives	9
CHAPTER 3: Experimental section	10-13
3.1 Materials and methods	
_	10
3.1 Materials and methods	10
3.1 Materials and methods	10 10-11 11-12
3.1 Materials and methods	10 10-11 11-12 12
3.1 Materials and methods	10 10-11 11-12 12
3.1 Materials and methods 3.2 Synthesis of gelator molecule G10 3.3 Preparation of gels 3.4 Gel melting temperature 3.5 Rheological properties of gel	10 10-11 11-12 12 12
3.1 Materials and methods	10 10-11 11-12 12 13
3.1 Materials and methods	1010-1112121313
3.1 Materials and methods 3.2 Synthesis of gelator molecule G10 3.3 Preparation of gels 3.4 Gel melting temperature 3.5 Rheological properties of gel 3.6 Morphology of gel 3.7 Drug encapsulation and release study  CHAPTER 4: Results and discussions	1010-1112121313
3.1 Materials and methods 3.2 Synthesis of gelator molecule G10 3.3 Preparation of gels 3.4 Gel melting temperature 3.5 Rheological properties of gel 3.6 Morphology of gel 3.7 Drug encapsulation and release study  CHAPTER 4: Results and discussions 4.1 Synthesis and Characterizations	1010-111212131314-4014
3.1 Materials and methods 3.2 Synthesis of gelator molecule G10 3.3 Preparation of gels 3.4 Gel melting temperature 3.5 Rheological properties of gel 3.6 Morphology of gel 3.7 Drug encapsulation and release study  CHAPTER 4: Results and discussions 4.1 Synthesis and Characterizations 4.2 Reaction Scheme.	1010-111212131314-4014
3.1 Materials and methods 3.2 Synthesis of gelator molecule G10 3.3 Preparation of gels 3.4 Gel melting temperature 3.5 Rheological properties of gel 3.6 Morphology of gel 3.7 Drug encapsulation and release study  CHAPTER 4: Results and discussions 4.1 Synthesis and Characterizations 4.2 Reaction Scheme. 4.3 Solubility and gelation behavior of G10	1010-111212131314-401414

4.7 Characterizations	19-23
4.8 Rheological Analysis	23-27
4.9 PXRD Analysis	28-29
4.10 Thermogravimetric Analysis	29-30
4.11 FE-SEM Analysis	30-32
4.12 Self-healing and injectability of <b>G10-Dox</b> organogel	32-33
4.13 UV-Vis Spectra Analysis	33
4.14 Fluorescence Spectra Analysis	33-34
4.15 Visual and Fluorometric Analysis with Fluoride ions.	34-35
4.16 Cell Viability Assay	35-36
4.17 Encapsulation efficiency and drug release study	36-39
CHAPTER 5: Conclusion and future scope	40
5.1 Conclusion	40
4.1 Future scope	40
References	41-44

# LIST OF FIGURES

Figure		Descr	iption		Page No
Figure 1.1	External	stimuli	inducing	sol-gel	2
	transition				
Figure 1.2	Classificat	ion of gels			3
Figure 1.3	Formation	of gel			3
Figure 1.4	Structures	of some r	epresentativo	e gelator	7
	molecules				
Figure 3.1	G10 organ	ogel forma	ation		11
Figure 3.2	G10-Dox	organogel	formation		12
Figure 4.1	Optimizati	on of gel	ation condi	tions of	16
	gelator mo	lecule G10	)		
Figure 4.2	Gelation 1	behavior o	of gelator i	nolecule	17
	G10 with t	ransition n	netal ions (Fe	$e^{2+}$ , $Co^{2+}$ ,	
	Ni <sup>2+</sup> , Cu <sup>2+</sup> ,	$Zn^{2+}$			
Figure 4.3	Gelation 1	behavior o	of gelator i	nolecule	18
	G10 with a	alkali meta	l ions (Li <sup>+</sup> , N	Na <sup>+</sup> , K <sup>+</sup> )	
Figure 4.4	Gelation 1	behavior o	of gelator i	nolecule	19
	G10 with p	ootassium s	salts of halide	e ions (F	
	, Cl <sup>-</sup> , Br <sup>-</sup> , I	-)			
Figure 4.5	Mass spect	trum of gel	lator molecu	le <b>G10</b>	19
Figure 4.6	<sup>1</sup> H NMR	spectrum	of gelator i	nolecule	20
	G10				
Figure 4.7	<sup>13</sup> C NMR	spectrum	of gelator r	nolecule	21
	G10				
Figure 4.8	IR spectru	m of gelate	or molecule	G10	22
Figure 4.9	IR spectra	of gelato	r molecule	<b>G10</b> and	22
	G10 xerog	el			
Figure 4.10	(a) Linear	viscoelast	ic (LVE) ra	inge and	23
	angular fr	requency	sweep (b)	of <b>G10</b>	
	organogel	at critical ş	gel concentra	ation	

Figure 4.11	(a) Linear viscoelastic (LVE) range and	23
	angular frequency sweep (b) of the most	
	stable G10 organogel	
Figure 4.12	(a) Linear viscoelastic (LVE) range and	24
	angular frequency sweep (b) of G10-Li	
	metallogel	
Figure 4.13	(a) Linear viscoelastic (LVE) range and	25
	angular frequency sweep (b) of G10-Na	
	metallogel	
Figure 4.14	(a) Linear viscoelastic (LVE) range and	25
	angular frequency sweep (b) of G10-K	
	metallogel	
Figure 4.15	Strain sweep (thixotropic) experiments of	26
	(a) G10 organogel, (b) G10-Li metallogel,	
	(c) G10-Na metallogel, and (d) G10-K	
	metallogel	
Figure 4.16	(a) Linear viscoelastic (LVE) range and	27
	angular frequency sweep (b) of G10-Dox	
	organogel	
Figure 4.17	Strain-sweep (thixotropic) experiment of	27
	G10-Dox organogel	
Figure 4.18	PXRD spectra of (a) gelator G10 and (b)	28
	G10 xerogel	
Figure 4.19	PXRD spectra of G10-Dox xerogel	29
Figure 4.20	TGA analysis of gelator molecule G10	29
Figure 4.21	TGA analysis of (a) G10 and (b)G10-	30
	<b>Dox</b> xerogel	
Figure 4.22	FE-SEM image of gelator molecule G10	31
Figure 4.23	FE-SEM images of (a), (b) G10 xerogel,	31
	(c) G10-Na xerogel, and (d) G10-K	
	xerogel	
Figure 4.24	FE-SEM image of <b>G10-Dox</b> xerogel	32

Figure 4.25	Images showing the self-healing property	32
	of G10-Dox organogel	
Figure 4.26	Images showing the injectability of G10-	33
	<b>Dox</b> organogel	
Figure 4.27	UV-Visible spectrum of G10	33
Figure 4.28	Fluorescence spectrum of G10	34
Figure 4.29	Images showing the gel-to-sol transition	34
	of G10 organogel after the addition of	
	fluoride ions.	
Figure 4.30	Changes in the emission spectra of G10	35
	upon the addition of halide ions	
Figure 4.31	Determination of cytotoxicity through	36
	MTT assay of G10 in HEK293 cell line	
Figure 4.32	(a) UV-Vis spectra of different	37
	concentration solutions of doxorubicin in	
	PBS buffer and (b) Calibration curve	
Figure 4.33	Evaluation of encapsulation efficiency of	37
	doxorubicin from UV-Vis spectroscopy	
Figure 4.34	Images showing the drug delivery of	38
	doxorubicin after the addition of PBS	
	buffer to G10-Dox organogel	
Figure 4.35	(a) UV-Visible spectra and (b) release	38
	profile of time-dependent drug release	
	from <b>G10-Dox</b> organogel at pH 7.4	
Figure 4.36	(a) UV-Visible spectra and (b) release	39
	profile of time-dependent drug release	
	from <b>G10-Dox</b> organogel at pH 4.8	

# LIST OF TABLES

Table	Description	Page No.
<b>Table 4.1</b>	Solubility of gelator molecule G10 in	16
	various solvents	
Table 4.2	Optimization table of gelation conditions	16
	of gelator molecule G10	
Table 4.3	Gelation behavior of gelator molecule G10	17
	with transitional metal ions (Fe <sup>2+</sup> , Co <sup>2+</sup> ,	
	$Ni^{2+}, Cu^{2+}, Zn^{2+})$	
Table 4.4	Gelation behavior of gelator molecule G10	18
	with alkali metal ions (Li+, Na+, K+)	
Table 4.5	Gelation behavior of gelator molecule G10	19
	with potassium salts of halide ions (F-, Cl-,	
	Br <sup>-</sup> , I <sup>-</sup> )	

# LIST OF SCHEME

Scheme	Description	Page No.
Scheme 4.1	Synthetic route for G10 synthesis	15

# **NOMENCLATURE**

δ	Chemical Shift (NMR)		
°C	Degree Centigrade		
g	gram		
mg	Milli gram		
mL	Milli Litre		
$\mu L$	Micro Litre		
mmol	Milli Mole		
mol	Mole		
ppm	Parts per million		
%	Percentage		
h	Hours		

# **ACRONYMS**

ACN Acetonitrile CHCl<sub>3</sub> Chloroform

**DCM** Dichloromethane

DMF N, N-DimethylformamideDMSO Dimethylsulphoxide

**ESI-MS** Electron Spray Ionization-Mass

Spectrometry

**EtOH** Ethanol

FT-IR Fourier Transform-Infrared

HCl Hydrochloric acid

H<sub>2</sub>O Water

LMWGs Low molecular weight gelators

MeOH Methanol

NMR Nuclear Magnetic Resonance

N<sub>2</sub> Nitrogen

**PBS** Phosphate-buffered saline

**PXRD** Powder X-ray Diffraction

**TGA** Thermogravimetric Analysis

UV-Vis Ultraviolet-Visible

# CHAPTER 1

# **INTRODUCTION**

#### 1.1 General Introduction

Gels are unique substances that have the appearance of solids when actually they consist mainly of liquid. Gels are usually constituted of two major components: a solvent and a gelator. Gelators are molecules that can self-assemble into fibrous, three-dimensional networks by noncovalent interactions in the solvent medium. This network traps the solvent and confers the solid-like characteristics to the gel. The solvent typically makes up approximately one hundred times the weight of the gelator and gives the gel its viscoelastic properties.<sup>2</sup> Gel formation is promoted by a range of non-covalent interactions between the selfassembled molecules of the gelator, namely  $\pi$ - $\pi$  stacking, hydrogen bonding, intercolumnar stacking, dipole-dipole interactions, and hydrophobic forces.<sup>3</sup> Gelation is initiated through the aggregation of gelator molecules into one-dimensional fibrils that become entangled and enmesh solvent molecules in the network. Effective gelation depends on a delicate balance between the dissolution propensity of the gelator and its aggregation propensity.<sup>4</sup> The chemical makeup of the gelator and the solvent is important to the process of gelation. Functional groups on these molecules have interactive sites for self-organization and interaction with the solvent. Such structural changes on the chemical level of the gelator will introduce sizeable variations in the characteristics of the resulting gel, enabling molecular-level fine-tuning to a desired application. <sup>5</sup> The concentration of the gelator, temperature, pH, solvent, etc, also influences gel formation.

Gels are susceptible to external stimuli like temperature, pressure, pH, light, etc., because any alteration in these conditions can induce changes in the various weak non-covalent interactions in the gel network (**Figure 1.1**).<sup>6</sup> This will lead to minute changes in the aggregation and morphology, and further to gel-to-sol transition. These properties can equip these materials for suitable applications in different sectors.<sup>7</sup>

Many gels are reported to have properties like biocompatibility, conductivity, and external stimuli-induced enhanced visual and mechanical properties, which make them potential candidates for drug delivery, energy storage, sensors, etc.<sup>8</sup>

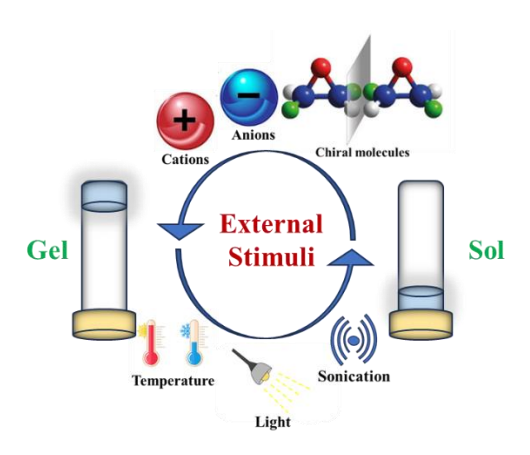


Figure 1.1: External stimuli inducing sol-gel transition

#### 1.2 Classification of gels

The constituents of a gel are a 3-D network and the entrapped solvent in the network. They are categorized based on different criteria, such as the type of cross-linking of the 3-D network, their origin, the type of solvent present, and their constitution (Figure 1.2). Based on the origin, the gels are divided into natural and artificial, while the gels with natural origin are formed by weak noncovalent interaction, which makes them thermally reversible and are known as physical gels; the artificial gels can either be physical gels or chemical gels. Chemical gels are formed by the strong chemical cross-linking in the network, which makes them thermally irreversible. Based on the constitution, gels are classified into macromolecular and supramolecular. Macromolecular gels comprise polymers, while the latter are formed from low molecular weight compounds. Macromolecular gels can be physical or chemical, while supramolecular gels are physical. The solvent that the gel encompasses also makes another basis for the classification. Hydrogels contain water as the solvent, while organogels are formed when the gelators are dispersed in an organic solvent. Aerogels or xerogels use air as the medium.10

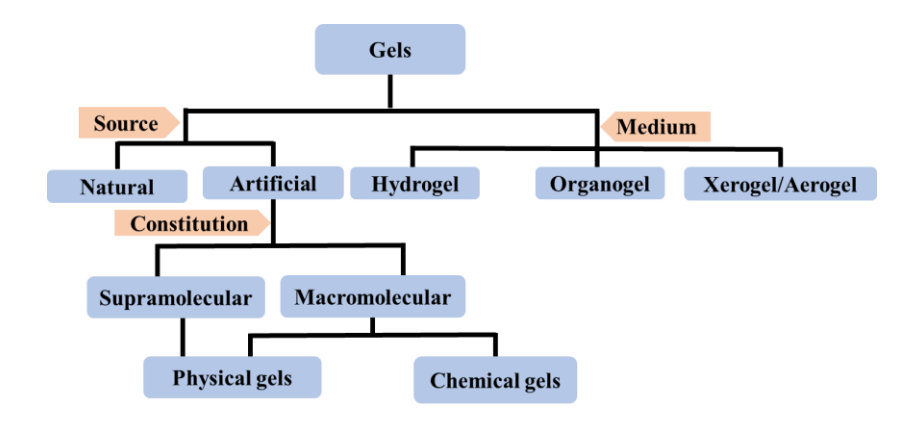


Figure 1.2: Classification of gels

# 1.3 Synthesis and Fabrication of Gels

A supramolecular gel is generally defined as a gel that is produced by noncovalent interactions between its component molecules to create a three-dimensional structure. Molecular gels, especially, are obtained from low molecular weight gelator molecules (LMWGs), which build up the structural backbone by self-organization through non-covalent forces like  $\pi$ - $\pi$  stacking, hydrogen bonding, intercolumnar stacking, and so on. The process of gelation of LMWGs is dynamic in nature. The gelator molecules first are dissolved in a state of high solubility, and this can be done either by increasing the temperature or a good solvent. A transition to lower solubility state is then triggered either by decreasing the temperature or by adding a poor solvent. This transformation induces the self-organization of gelator molecules. These molecules nucleate and structure into one-dimensional nanofibrils. When the fibrils attain a critical length, they start to crosslink, generating a three-dimensional network that traps the solvent, thus producing the gel (**Figure 1.3**).  $^{12}$ 

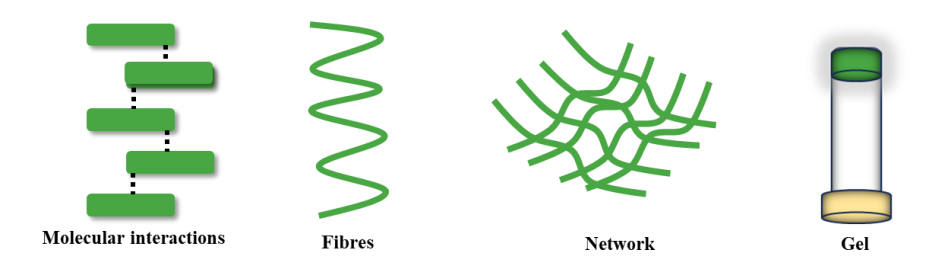


Figure 1.3: Formation of gel

# 1.4 Properties and characterization of gels

upramolecular gels are formed by the spontaneous assembly of small molecules possessing specific functional groups in their chemical backbones. Because these molecules differ in their functionalities, aspects such as the selection of solvent, concentration required for gelation, and mechanism of gelation may be variable. In order to find out gel formation, solutions of different concentrations of the gelator molecules are examined in a suitable solvent under standard conditions to form a stable gel. The minimum concentration through which the gelator molecules can come together to form a stable gel network is referred to as the critical gel concentration (CGC). Above or at the CGC, the molecules interact and organize into the gel state, and below this critical value, the molecules remain uniformly distributed within the solvent.<sup>13</sup>

Several methods are employed to study the chemical, physical, mechanical, and structural properties of gels. Nuclear Magnetic Resonance (NMR) spectroscopy, in fact, is used to study the interactions between the solvent and gelator, gelator molecules, and the gelator and any external guest molecules. Peak shifts, peak broadening, and appearance or disappearance of peaks are observed, and from these, the nature of these interactions can be understood.<sup>14</sup>

Supramolecular gelation is analyzed through Fourier Transform Infrared (FT-IR) spectroscopy, which provides useful insight into the self-organization of gelator molecules and their non-covalent interactions. By interpreting variations in peak intensity and shifts in the characteristic functional group signals in the IR spectra of both the gelator molecule and the xerogel, these functional groups' interactions can be understood more clearly. Y-ray diffraction techniques are also used to understand the crystallinity and orientation of the gelator molecules. The orientation of the gelator molecules by non-covalent interactions can be analyzed from the interplanar distances obtained from the X-ray diffraction pattern. In the content of the selection of the gelator molecules obtained from the X-ray diffraction pattern.

The gel's mechanical properties, including its strength and gel-sol transition behaviour, are analyzed through rheology. Small deformation rheology is employed in the viscoelastic region of the gel to assess these properties. In amplitude oscillatory shear measurements, G' measures the material's stiffness or solid-like behavior, and G" the flow or liquid-like behavior of the material. The material behaves more like an elastic solid when G' is greater than G" and more like a viscous liquid when G" is greater than G'. Plotting the moduli against strain reveals the linear viscoelastic region, where G' and G" are constant irrespective of shear strain. Furthermore, the behavior of the gel at both short and long time scales can be observed by plotting the moduli against frequency. Thixotopic behaviour is also exhibited by some gels, in which the solid-like behavior of the gel decreases over time by applying constant strain, and it is recovered back to a solid state by removing the strain.<sup>17</sup>

FE-SEM (Field Emission-Scanning Electron Microscopy) is used to understand the microscopic structures in the morphology of the self-assembled systems. The fibrillar network formed by the gelator molecules, which immobilizes the solvents, has a size range from several nanometers to a few tens of micrometers and can be elucidated using this technique. <sup>18</sup> EDS (Energy dispersive X-ray spectroscopy) is a microanalytical technique used to identify and quantify the elemental distribution in the gel matrix.

The thermal stability and decomposition of the gelator and the xerogel under controlled temperature conditions are evaluated using TGA (Thermogravimetric Analysis).

# 1.5 Drug delivery

Researchers are focused on developing materials with high drug loading efficiency and controlled release, maintaining the drug concentration over an extended period. Gels are utilized as drug delivery systems because they can encapsulate and release bioactive compounds in a controlled and sustained manner. They are advantageous as the delivery can be optimized to local or targeted sites with minimum side effects

and enhanced efficacy.<sup>19</sup> The controlled release is possible due to their sensitivity to external stimuli like pH, temperature, redox environment, etc. This makes them efficient "smart materials" that can deliver the cargo to specific sites with improved efficacy. Furthermore, gel formulations with biodegradable or biocompatible materials enhance their safety profile as they can degrade into nontoxic materials over time.<sup>20</sup>

# CHAPTER 2

### 2.1 Literature review and motivation

Organogels are formed by immobilizing an organic liquid within the network formed by low molecular weight gelator molecules. Although several gelator molecules have been reported with various characteristic functional groups that can participate in non-covalent interactions, which finally aid in forming gels, the exact structural requirement for a molecule to gel an organic liquid is not yet predictable.<sup>21</sup> Molecules dissolved in an organic solvent can arrange themselves in various ways depending on the conditions. They might create highly ordered crystalline structures, randomly ordered aggregates that produce an amorphous precipitate, or an intermediate arrangement that gives rise to the formation of a gel. The nature of the arrangement varies with factors such as the molecular structure, the type of solvent used, and the surroundings. A delicate balance exists between the solubilization and crystallization to form a gel.<sup>22</sup>

Figure 1.4: Structures of some representative gelator molecules

Different functional groups like amide, imine, carboxylic acid, and heterocyclic rings in the gelator molecule play a crucial role in noncovalent interactions and further self-organization. **Figure 1.4** shows some previously reported gelator molecules with these functional groups. The imine group has received attention due to its binding properties towards anions and cations, and several approaches have been done to develop stimuli-responsive organogelators with this functional group.<sup>23,24</sup> Most Schiff base gelators are designed by introducing gel-

promoting units such as urea, sugar, and cholesterol into their structure. This makes the synthesis process relatively complicated and impedes its practical application. Wang et al designed and synthesised a low molecular weight Schiff base organogelator molecule in a single step process which have multiple stimuli response especially for fluoride detection.<sup>25</sup> These simple gel-forming moieties are more desirable due to their easy synthesis from simple and readily available materials.

In biomedicine, self-assembled systems have gained prominence mainly due to their potential usage in drug delivery. Assembled systems, including lipid nanoparticles, 26 polymeric materials, 27 and biomacromolecules, 28 have been successfully used for drug delivery to specific sites due to their ideal response to several external stimuli. Thakur et al have developed a pH-responsive dual cross-linked G-quadruplex-based hydrogel for the effective drug delivery of doxorubicin. 29 Even though drug delivery systems based on hydrogels are well established, researchers are developing the field of organogels for their potential applications in drug delivery.

Zare et al used a redox-responsive organogelator molecule based on cysteine derivatives, which have disulfide bonds, as a drug delivery system for doxorubicin.<sup>30</sup> Ritik et al have fabricated a Ru-based metallogel of a novel gelator molecule A2, which demonstrated prolonged, efficient drug delivery in targeted cancerous cells based on the difference between the pH in healthy and cancerous cells.<sup>31</sup> The gelator molecule used in the drug delivery system must be biocompatible to ensure it does not damage healthy cells and provide an improved safety profile for prolonged use.

In recent years, there has been a lot of interest in imidazole-based compounds due to their beneficial qualities, such as high tissue permeability, low frequency of toxic or adverse effects, and bioavailability, which makes them potential candidates for medicinal chemistry and material science.<sup>32</sup> This work synthesized and employed a novel imidazole-based Schiff base gelator molecule to prepare an

organogel in a DMSO-H<sub>2</sub>O mixture. The organogel fabricated had an excellent stimulus response towards various cations and anions. Further, the organogel is used as a drug delivery system for the drug doxorubicin, as it has a high biocompatibility.

# 2.2 Objectives

- Synthesise a low molecular weight gelator molecule through a simple one-step process using easily accessible starting materials.
- Investigate its gelation properties, including the conditions under which gel formation occurs and the metallogel formation.
- Examine the mechanical, morphological, and chemical properties of the organogel and alkali metal ion-based metallogel.
- Explore potential applications of the gel, focusing on areas such as drug delivery, which analyzes the gel's drug-loading efficiency and the gel's sensing ability.

# CHAPTER 3

#### **EXPERIMENTAL SECTION**

#### 3.1 Materials and Methods

The solvents and chemicals used in this work were purchased from Sigma-Aldrich, TCI, BLD Pharm, Finar, and Avra. Infrared (FTIR) spectra were recorded employing a Bruker Tensor 27 FTIR Spectrometer in the range of 4000–500 cm<sup>-1</sup>. Electrospray ionization mass spectra (ESI-MS) were recorded using a MicrOTOF QII system with a Bruker Daltonics Apollo II ESI source. Nuclear magnetic resonance (NMR) spectra were obtained on an AVANCE NEO Ascend 500 BioSpin International AG Bruker spectrometer tetramethylsilane (TMS) as the internal standard and DMSO-d<sub>6</sub> solvent at room temperature. Mechanical and thixotropic properties of the gels were determined on an Anton Paar Physica MCR 301 rheometer using a 25 mm parallel plate geometry with a 0.5 mm gap at 25 °C. Morphology of the gelator and xerogels was analyzed by a Supra55 Zeiss field emission scanning electron microscope (FE-SEM). Powder X-ray diffraction (PXRD) patterns of the gelator and xerogels were obtained with a Rigaku SmartLab automated multipurpose diffractometer. Thermogravimetric analysis (TGA) was conducted in a Mettler Toledo Thermal Analyzer in the temperature range of 30–800°C with a heating rate of 10 °C/min under nitrogen. Fluorescence emission spectra of the gelator were obtained on a Horiba Fluoromax-4 spectrofluorometer. UVvisible absorption spectra and drug release profiles were measured on a Varian Cary 100 UV-Vis spectrophotometer.

# 3.2 Synthesis of gelator 5-(((1H-imidazol-2-yl) methylene)amino)isophthalic acid) (G10)

In a round-bottom flask, 0.18 g (1 mmol) of 5-amino isophthalic acid was suspended in 20 mL of methanol, along with 0.096 g (1 mmol) of 2-imidazole carboxaldehyde, and the mixture was stirred. The reaction mixture was heated at 60 °C and refluxed for 24 hours. After the

reaction, the resulting precipitate was filtered through filter paper, washed with methanol, and dried in an oven. The desired gelator compound was obtained as a white powder (0.21 g, 83% yield).

# 3.3 Preparation of gels

#### 3.3.1 Preparation of G10 organogel and its metallogels

For the formation of **G10** organogel, 0.046 mmol (12 mg) of **G10** was dissolved in 500 μL of DMSO, and an equal volume of Milli-Q water was added to the solution. A yellow-colored stable organogel is obtained after 5 minutes. To fabricate the metallogel of **G10** with transition metals, 0.046 mmol (12 mg) of **G10** was dissolved in 500 μL of DMSO, and 0.05 mmol of **perchlorate salt** solution of Fe<sup>2+</sup>, Co<sup>2+</sup>, Ni<sup>2+</sup>, Cu<sup>2+</sup>, and Zn<sup>2+</sup> in 500 μL of Milli-Q water was added to it. **G10** was found not to form metallogels with transition metals. Further metallogels of **G10** with alkali metals were prepared by solubilizing 0.046 mmol of **G10** in 500 μL DMSO and adding 0.05 mmol of **chloride salt** solution of Li<sup>+</sup>, Na<sup>+</sup>, and K<sup>+</sup> in 500 μL Milli-Q water to it. Stable metallogels of Li<sup>+</sup>, Na<sup>+</sup>, and K<sup>+</sup> were obtained. The formation of gels was confirmed by the conventional tube inversion method (**Figure 3.1**).

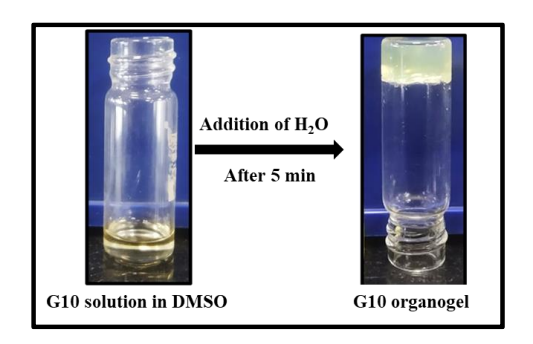


Figure 3.1: G10 organogel formation

# 3.3.2 Preparation of G10 metallogels with halide ions of potassium salt

For the formation of **G10** metallogels with halide ions of potassium salt, 0.046 mmol (12 mg) of G10 was dissolved in 500 µL DMSO, and a 0.05 mmol solution of potassium salts F-, Cl-, Br-, and I<sup>-</sup> in 500 µL Milli-Q water was added to it. Stable gels were formed except for F<sup>-</sup> salt after 5

minutes. The gel formation was confirmed by the conventional test tube inversion method.

# 3.3.3 Preparation of G10-Dox organogel

To form **G10-Dox** organogel, 0.046 mmol (12mg) of **G10** was dissolved in 500  $\mu$ L DMSO, and 1 mg of Dox dissolved in 500  $\mu$ L Milli-Q water was added. After 5 minutes, sable organogel was obtained, and the gel formation was confirmed by the conventional test tube inversion method (**Figure 3.2**).

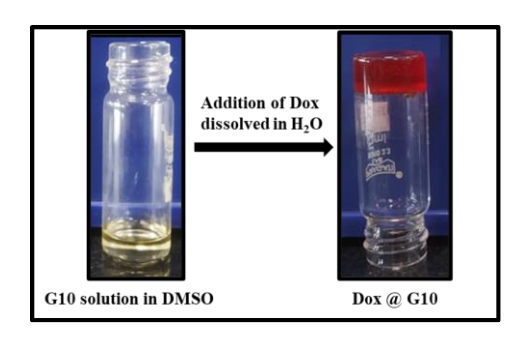


Figure 3.2: G10-Dox organogel formation

# 3.4 Gel melting temperature (T<sub>gel</sub>)

The melting temperature of the gel (Tgel) and temperature-dependent sol-gel phase transition behavior were investigated in a silicone oil bath. A 46 mM G10 organogel prepared in a 1:1 v/v solution of DMSO and water was filled in a 5 mL glass vial, and the temperature was monitored by a thermometer. A steel ball was put on the gel, and the vial was placed in the oil bath. With the rise in temperature, the commencement of melting of the gel was signaled by the displacement of the steel ball. The heating was arrested at this stage, and the respective temperature was noted. After five minutes, the system reverted back to the gel form.

# 3.5 Rheological properties of gels

The mechanical properties, strength, and sol-gel behavior of the transition were characterized under oscillatory rheology. Viscoelastic character was ascertained from the measurement of viscoelastic storage (G') and loss (G") moduli at 1% strain. Thixotropic behavior or strain response time dependency was found out with strain sweep experiments

from a minimum of 1% to a maximum of 100% strain. The sample of gel was deposited directly onto the rheometer stage with a spatula.

# 3.6 Morphology of gels

The morphological properties of the gelator and the organogel were analysed using field-emission scanning electron microscopy (FE-SEM). A small quantity of gel was placed on the glass slide, dried, and coated with gold film to make the sample.

# 3.7 Drug encapsulation and release study

To formulate the **G10-Dox** organogel, 1 mg of doxorubicin in 500  $\mu$ L Milli-Q water was mixed with 12 mg of **G10** in 500  $\mu$ L DMSO. Free drug molecules were eliminated by washing with pH 7.4 PBS buffer and monitoring the absorbance of the supernatant obtained after washing by UV-Visible spectroscopy. The quantity of drug entrapped in the gel matrix was calculated by subtracting the quantity of drug remaining in supernatant from the initial quantity added. The encapsulation efficiency was subsequently calculated from the equation below,

Encapsulation efficiency (%) = 
$$\frac{Amount\ of\ drug\ present\ after\ washing}{Drug\ taken\ initially}$$
 x
$$100$$

Drug release from **G10-Dox** organogel was analyzed in neutral pH 7.4 and acidic pH 4.8, imitating the tumour environment. 1 mL of gel was taken in a glass vial, and 3 mL of PBS buffer was added and kept at room temperature for 90 hours. At the same 10-hour interval, 400  $\mu$ L of supernatant solution was removed from the vial and exchanged with fresh PBS buffer solution. The amount removed was analyzed by UV-Visible spectroscopy to observe the release of the drug, and the equation below was utilized to measure the drug released

Drug released = 
$$\frac{C_1 - C_t}{C_1} \times 100$$

where  $C_1$  and  $C_t$  are the absorbance of the drug taken initially and the absorbance at time interval t.

# CHAPTER 4

# **RESULTS AND DISCUSSIONS**

# 4.1 Synthesis and characterization

The gelator molecule **G10** was successfully synthesized and characterized. It was formed by the imine bond formation between 5-amino isophthalic acid and 2-imidazole carboxaldehyde in the presence of methanol (**Scheme 4.1**) as a white-colored solid product. Characterization techniques such as <sup>1</sup>H NMR, <sup>13</sup>C NMR, and FT-IR spectroscopy were used to confirm the synthesis.

#### 4.2 Reaction Scheme

# Synthesis of G10

Scheme 4.1: Synthetic route for G10 synthesis

# 4.3 Solubility and gelation behavior of gelator molecule G10

The solubility of gelator molecule **G10** has been checked in various solvents. It was found to be readily soluble in DMSO and became soluble upon heating in DMF, as shown in the table below (**Table 4.1**). The critical gel concentration of the organogel of gelator molecule **G10** was determined by preparing different concentration solutions of gelator **G10** in DMSO, into which water was added, where the DMSO: H<sub>2</sub>O volume ratio is 1:1 (**Table 4.2**). A 42.4 mM solution of gelator molecule **G10**, prepared with a 1:1 volume ratio of DMSO and water, was observed to form a weak organogel. As a result, the molecule's critical gel concentration (CGC) was determined to be 42.4 mM. The compound formed a strong transparent gel at 46.3 mM concentration. The

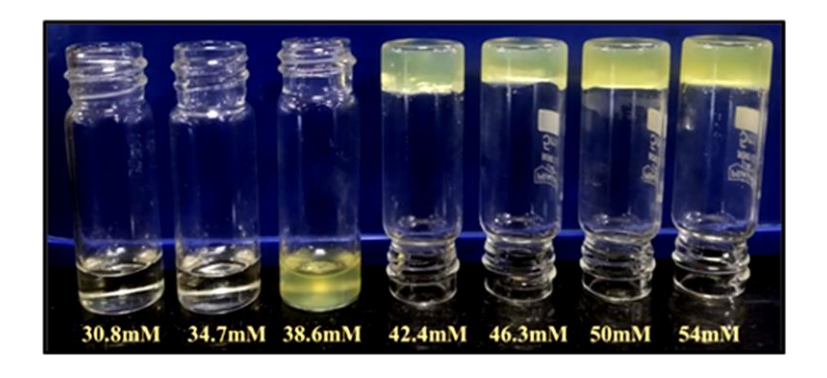
formation of the gel was confirmed using the standard test tube inversion method (**Figure 4.1**).

Table 4.1: Solubility of gelator molecule G10 in various solvents

Solvent	Solubility	Gelation	Solvent	Solubility	Gelation
Methanol	Insoluble	-	CHCl <sub>3</sub>	Insoluble	-
DMSO	Soluble	Gelation	H <sub>2</sub> O	Insoluble	-
Acetone	Insoluble	-	DMF	Soluble	-
Ethanol	Insoluble	-	Hexane	Insoluble	-
DCM	Insoluble	-	ACN	Insoluble	-

**Table 4.2:** Optimization table of gelation conditions of gelator molecule **G10** 

Concentration	DMSO / H <sub>2</sub> O	Gelation
30.8 mM	$500~\mu L/500~\mu L$	No
34.7 mM	$500~\mu L/500~\mu L$	No
38.6 mM	500 μL / 500 μL	No
42.4 mM	500 μL / 500 μL	Yes
46.3 mM	500 μL / 500 μL	Yes (Strong gel)
50 mM	500 μL / 500 μL	Yes (Strong but opaque gel)
54 mM	500 μL / 500 μL	Yes (Strong but opaque gel)



**Figure 4.1.** Optimization of gelation conditions of gelator molecule **G10** 

### 4.4 Gelation behavior of G10 with transition metals

It is fascinating to observe the gelation properties of gelator **G10** with transition metal ions, as it combines the structural versatility of metal ligand chemistry with the soft nature of gels. The gelation ability of gelator molecule **G10** was checked with various transition metal salts. The procedure for forming the metallogels was adding 0.5 mmol solutions of perchlorate salts of Fe<sup>2+</sup>, Co<sup>2+</sup>, Ni<sup>2+</sup>, Cu<sup>2+</sup>, and Zn<sup>2+</sup> in 500  $\mu$ L of Milli-Q water to a 0.046 mmol (12 mg) solution of the gelator molecule **G10** in 500  $\mu$ L of DMSO. However, gel formation was not observed with any of the salts. (**Table 4.3**) and (**Figure 4.2**).

**Table 4.3:** Gelation behavior of gelator molecule **G10** with transitional metal ions (Fe<sup>2+</sup>, Co<sup>2+</sup>, Ni<sup>2+</sup>, Cu<sup>2+</sup>, Zn<sup>2+</sup>)

mmol of G10	Metal ion	DMSO:	Gelation
(500 μL	(0.5 mmol in 500 μL	H <sub>2</sub> O	
DMSO)	H <sub>2</sub> O)		
0.046	Fe <sup>2+</sup>	1:1	No gel
0.046	Co <sup>2+</sup>	1:1	No gel
0.046	Ni <sup>2+</sup>	1:1	No gel
0.046	Cu <sup>2+</sup>	1:1	No gel
0.046	$Zn^{2+}$	1:1	No gel

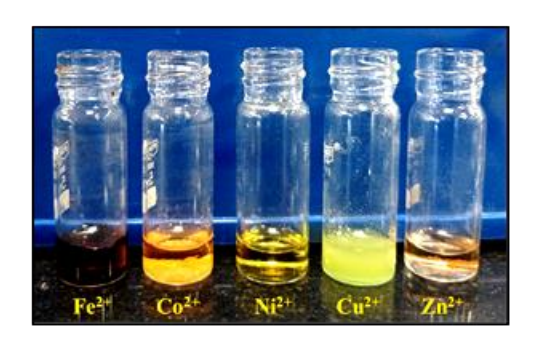


**Figure 4.2:** Gelation study of gelator molecule **G10** with transition metal ions (Fe<sup>2+</sup>, Co<sup>2+</sup>, Ni<sup>2+</sup>, Cu<sup>2+</sup>, Zn<sup>2+</sup>)

# 4.5 Gelation behavior of G10 with alkali metals

Alkali metal ions generally play an vital role in gel formation as they tend to interact with functional groups present in gelator molecules, triggering self-oorganization into a gel network. Therefore, the gelation ability of gelator molecule **G10** was checked with various alkali metal ions. The **G10** metallogels with alkali metals were prepared by uniformly adding 0.5 mmol solutions of chloride salts of Li<sup>+</sup>, Na<sup>+</sup>, and K<sup>+</sup> in 500  $\mu$ L of Milli-Q water to a 0.046 mmol (12 mg) solution of the gelator molecule **G10** in 500  $\mu$ L of DMSO. Gel formation was observed with all metal salts, verified by the test tube inversion method (**Table 4.4**) and (**Figure 4.3**).

**Table 4.4:** Gelation behavior of gelator molecule **G10** with alkali metal ions (Li<sup>+</sup>, Na<sup>+</sup>, K<sup>+</sup>)

mmol of G10	Metal ion	DMSO:	Gelation
(500 μL	(0.5 mmol in 500	H <sub>2</sub> O	
DMSO)	μL H <sub>2</sub> O)		
0.046	Li <sup>+</sup>	1:1	Gel
0.046	Na <sup>+</sup>	1:1	Gel
0.046	K <sup>+</sup>	1:1	Gel

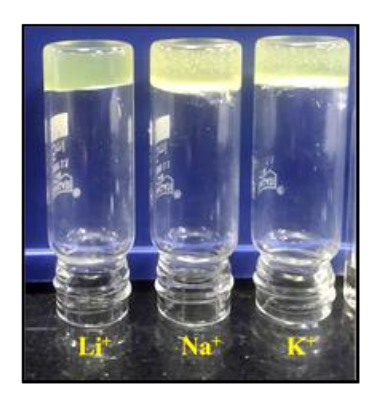


**Figure 4.3:** Gelation behavior of gelator molecule **G10** with alkali metal ions (Li<sup>+</sup>, Na<sup>+</sup>, K<sup>+</sup>)

# 4.6 Gelation behavior of G10 with potassium salts of halide ions

The gelation ability of gelator molecule **G10** was checked with halide ions. The **G10** metallogels with halide ion salts of potassium were prepared by adding 0.5 mmol solutions of potassium salts of  $F^-$ ,  $Cl^-$ ,  $Br^-$ , and  $I^-$  in 500  $\mu L$  of Milli-Q water to a 0.046 mmol (12 mg) solution of the gelator molecule **G10** in 500  $\mu L$  of DMSO. Gel formation was observed with all halide ions except for  $F^-$  salt, validated by the test tube inversion method (**Table 4.5**) and (**Figure 4.4**).

**Table 4.5:** Gelation behavior of gelator molecule **G10** with potassium salts of halide ions (F<sup>-</sup>, Cl<sup>-</sup>, Br<sup>-</sup>, I<sup>-</sup>)

mmol of G10	Halide ion	DMSO:	Gelation
(500 μL	(0.5 mmol in 500	H <sub>2</sub> O	
DMSO)	μL H <sub>2</sub> O)		
0.046	F	1:1	No gel
0.046	Cl	1:1	Gel
0.046	Br	1:1	Gel
0.046	I_	1:1	Gel

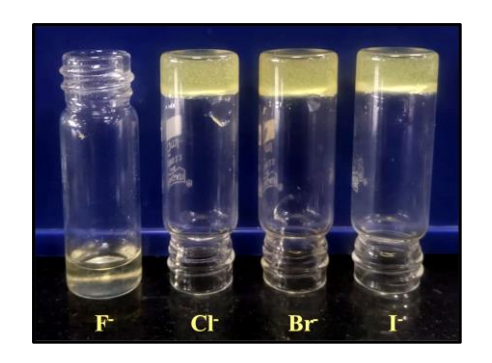


**Figure 4.4:** Gelation behavior of gelator molecule **G10** with potassium salts of halide ions (F<sup>-</sup>, Cl<sup>-</sup>, Br<sup>-</sup>, I<sup>-</sup>)

#### 4.7 Characterizations

# 4.7.1 Mass Spectra

The mass spectra of the synthesized compound were recorded using ESI-MS. The gelator molecule **G10** shows a molecular base peak at m/z = 258.0808 (in negative mode) (**Figure 4.5**).

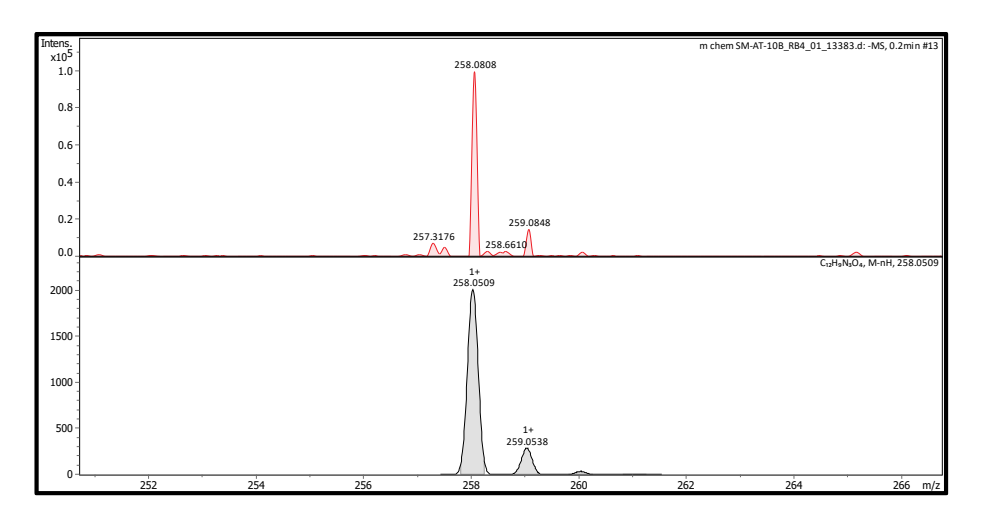


**Figure 4.5:** Mass spectrum of gelator molecule **G10**; ESI-MS (m/z) [C<sub>12</sub>H<sub>9</sub>N<sub>3</sub>O<sub>4</sub>-H]<sup>-</sup>: 258.0509; Found: 258.0808

# 4.7.2 NMR Spectra

The recorded NMR spectra of gelator molecule **G10** matched well with the proposed NMR spectra. The sample was prepared in DMSO-d<sub>6</sub>. The  $^{1}$ H NMR peaks are at  $\delta$  13.31 for the carboxylic acid proton,  $\delta$  8.50 for the imine proton,  $\delta$  8.35 for the deshielded aromatic proton by carboxylic acids,  $\delta$  7.98 for two aromatic protons,  $\delta$  7.37-7.33 for the imidazole ring proton, and  $\delta$  4.11 for the N-H proton of imidazole

(**Figure 4.6**). The <sup>13</sup>C NMR peaks are at  $\delta$  167.68 for the carboxylic acid carbon,  $\delta$  166.82 for the imine bond carbon,  $\delta$  152.97 for the aromatic carbon attached to nitrogen atom,  $\delta$  145.06 for the imidazole carbon attached to methylene group, peaks from  $\delta$  132.98-132.10 belong to the other aromatic carbons and  $\delta$  118.60 for the imidazole ring carbons (**Figure 4.7**).

<sup>1</sup>H NMR (400MHz, 298K, DMSO-d<sub>6</sub>) δ, ppm: 13.31 (s, 2H), 8.50 (s, 1H), 8.35 (s, 1H), 7.98 (s, 2H), 7.37 (m, 2H), 4.11(s, 1H). <sup>13</sup>C NMR (100MHz, 298K, DMSO-d<sub>6</sub>) δ, ppm: 167.68, 166.82, 152.97, 145.06, 132.98, 132.10, 126.05, 118.60.

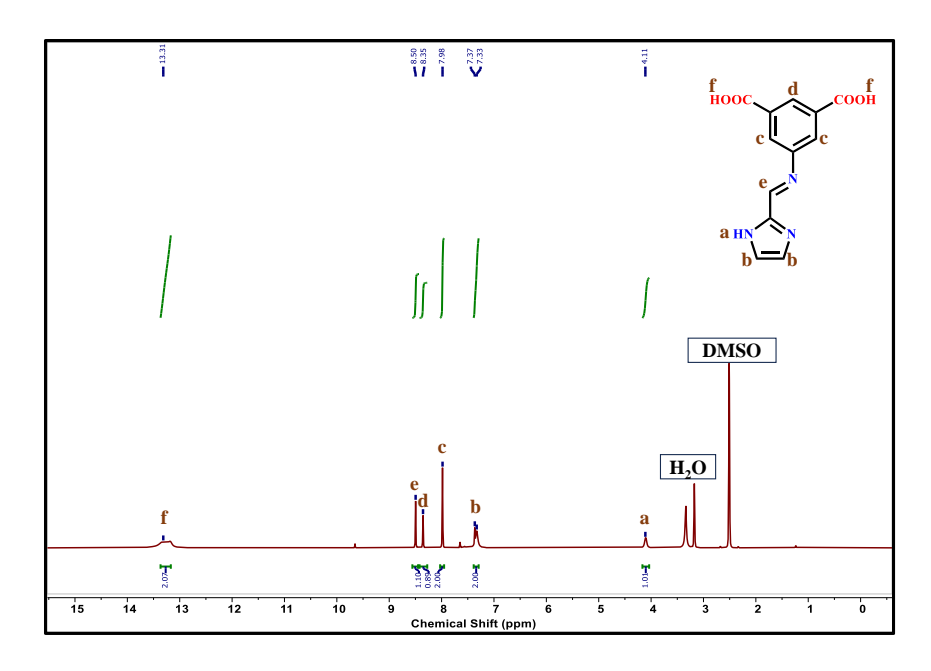


Figure 4.6: <sup>1</sup>H NMR spectrum of gelator molecule G10

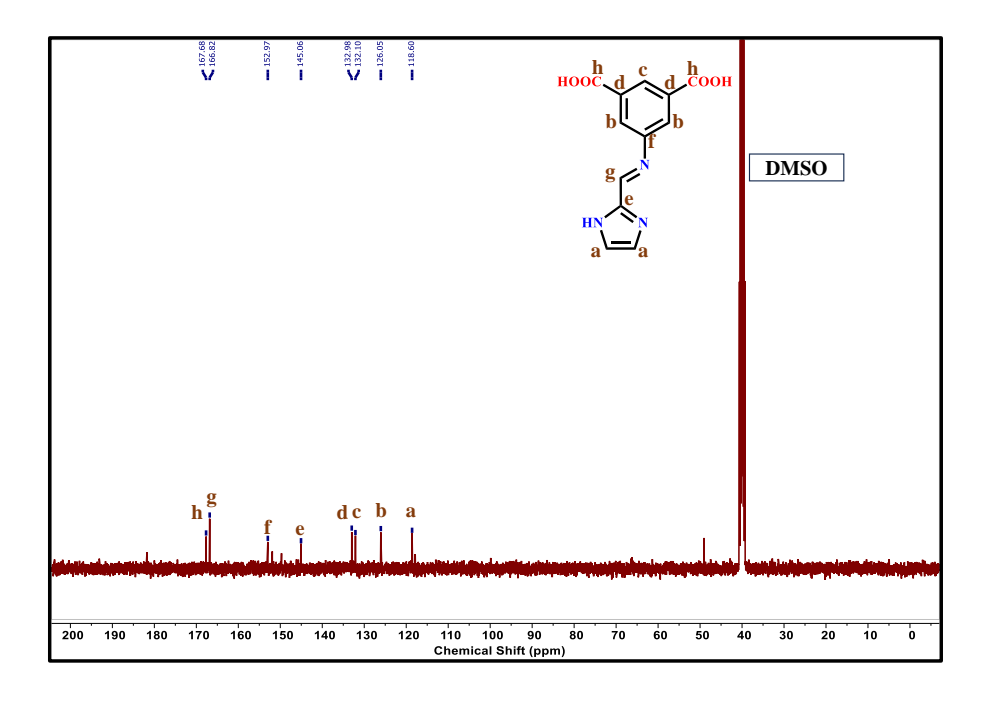


Figure 4.7: <sup>13</sup>C NMR spectrum of gelator molecule G10

# 4.7.3 FT-IR Spectra

The IR spectra of the compound, which were recorded, closely matched the signature bands of the functional groups of the gelator molecule **G10**. There was a fairly broad peak at 3500 cm<sup>-1</sup> showing N–H stretching. A rather broad peak at 2920 cm<sup>-1</sup> indicated the O–H stretching of carboxylic acid groups. A sharp peak at 1707 cm<sup>-1</sup> with high intensity corresponds to the C=O stretching vibration of carboxylic acid groups. A clear peak at 1616 cm<sup>-1</sup> was designated to C=N stretching of the imine group.<sup>34</sup> C=C stretching of the aromatic and imidazole groups was indicated by a peak at 1551 cm<sup>-1</sup>. O–H bending of the carboxylic acid groups occurred at 1404 cm<sup>-1</sup>. A clear peak at 1185 cm<sup>-1</sup> resulted from C–O stretching. Moreover, clear peaks at 870 cm<sup>-1</sup> and 750 cm<sup>-1</sup> were present for C–H bending vibrations (**Figure 4.8**).

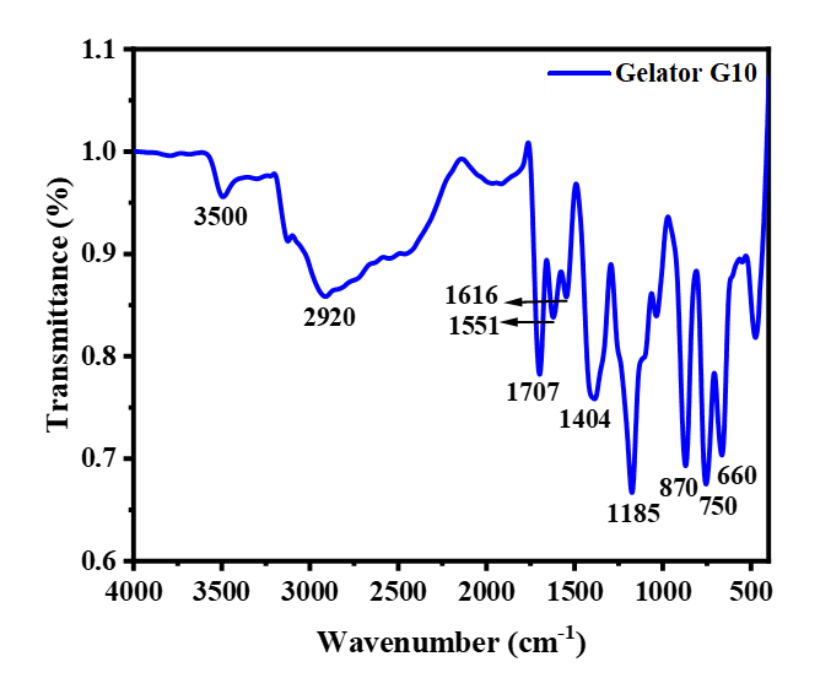


Figure 4.8: IR spectrum of gelator molecule G10

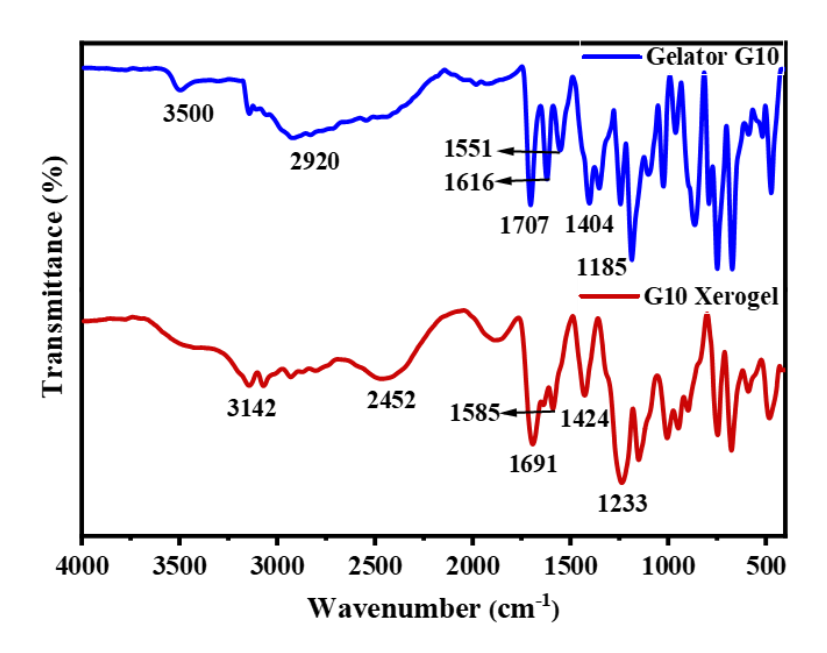


Figure 4.9: IR spectra of gelator molecule G10 and G10 xerogel

On the IR spectrum of the xerogel, the O–H stretching peak at 2452 cm<sup>-1</sup> was broader and more intense. The C=O stretching peak that was originally seen at 1707 cm<sup>-1</sup> broadened and shifted to a lower wavenumber at 1691 cm<sup>-1</sup>. This broadening and downward shift are due to increased hydrogen bonding within the gel phase. The C=N stretching signal was overlapping with the band of C=O stretching, whereas the

peak of N–H stretching was broader and more intensive. The C–O stretching peak at 1233 cm<sup>-1</sup> was also found to be broader. (**Figure 4.9**).

#### 4.8 Rheological Analysis

#### 4.8.1 G10 organogel and G10 metallogels with alkali metal ions

Rheological analyses offer valuable information about the mechanical and flow characteristics, helping to assess the strength and stability of the gels. The average storage modulus (G') of the critical and most stable gel of G10 was found to be  $6.72 \times 10^3$  and  $1.03 \times 10^4$  Pa (Figures 4.10 and 4.11), respectively. The storage modulus (G') was initially greater than the loss modulus (G") and remained linear. As the strain increased, the gel's behavior deviated from linearity, with a crossover occurring at a strain value of 36%. The graph of angular frequency versus storage and loss modulus further confirmed the gel's viscoelastic properties.

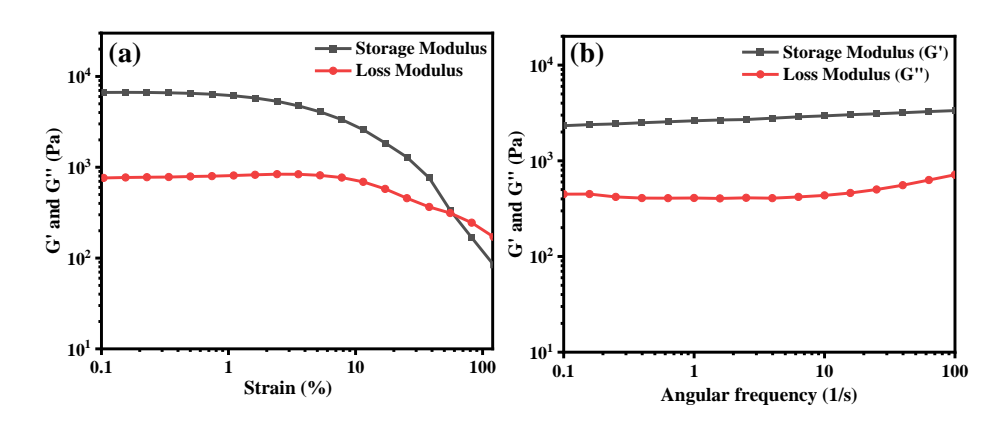


**Figure 4.10:** (a) Linear viscoelastic (LVE) range and angular frequency sweep (b) of **G10** organogel at critical gel concentration

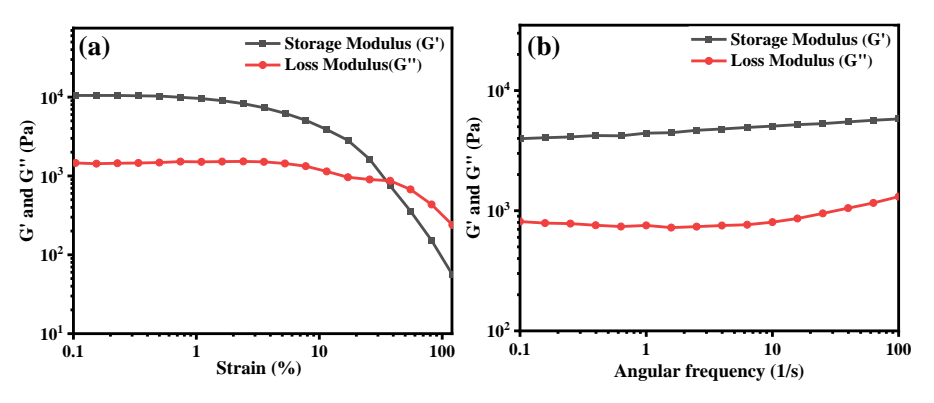


**Figure 4.11:** (a) Linear viscoelastic (LVE) range and angular frequency sweep (b) of the most stable **G10** organogel

It is interesting to observe how alkali metal ions can tune the mechanical stability of the **G10** gels. The alkali metal ion-based metallogels of **G10** with chloride salts of lithium, sodium, and potassium metals were prepared. The average storage modulus (G') was found to be  $1.47 \times 10^4$  Pa for **G10-Li** metallogel (Figure 4.12),1.01  $\times$  10<sup>4</sup> Pa for G10-Na metallogel (Figure 4.13), and  $1.1 \times 10^4$  Pa for **G10-K** metallogel (Figure 4.14) with a crossover point of 38%, 37%, and 55%, respectively. The storage (G') and loss (G') moduli of the metallogels were also measured by varying the angular frequency to confirm their viscoelastic properties. Rheological analysis of **G10** following the incorporation of alkali metal ions indicates a slight enhancement in both the storage modulus (G') and the loss modulus (G"). This suggests a modest increase in the material's elastic and viscous responses, which may be attributed to ionic interactions or structural modifications within the network induced by the presence of the alkali metal ions.

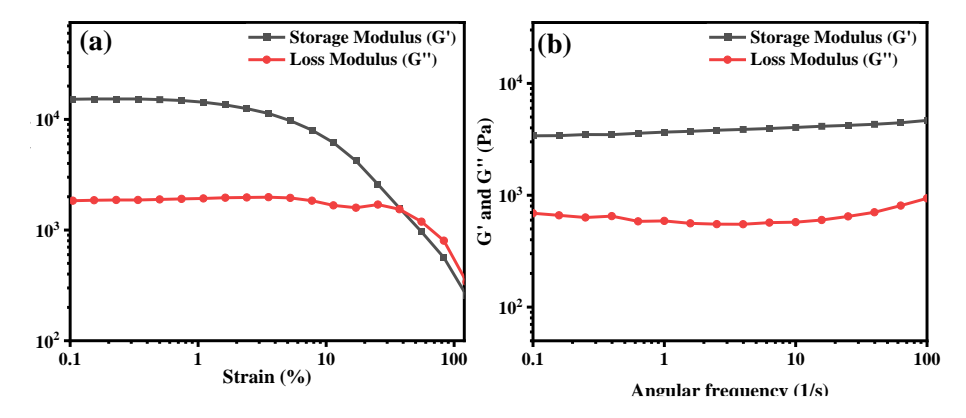


**Figure 4.12:** (a) Linear viscoelastic (LVE) range and angular frequency sweep (b) of **G10-Li** metallogel

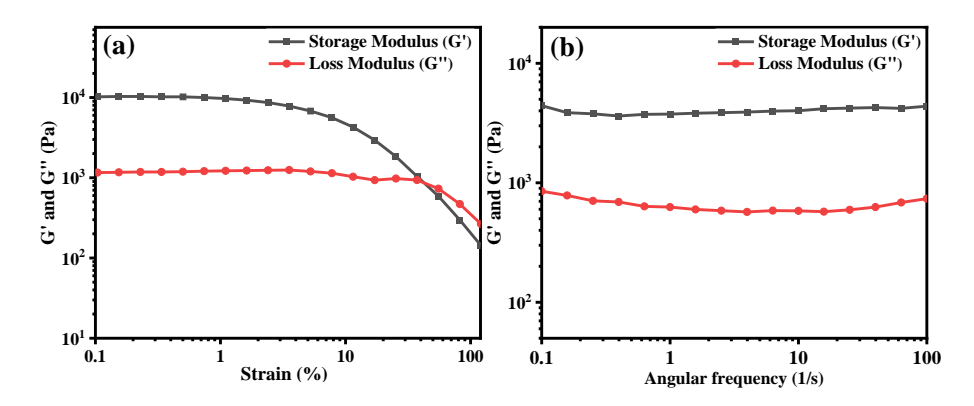


**Figure 4.13:** (a) Linear viscoelastic (LVE) range and angular frequency sweep (b) of **G10-Na** metallogel

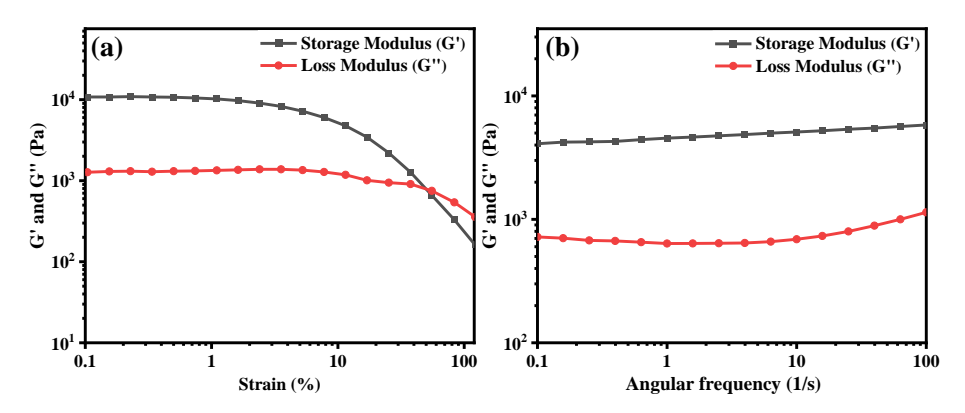


**Figure 4.14:** (a) Linear viscoelastic (LVE) range and angular frequency sweep (b) of **G10-K** metallogel

Thixotropic properties allow gels to flow smoothly under shear and quickly regain their structure when at rest, making them particularly useful in applications like coatings, catalysis, and drug delivery. Moreover, thixotropy improves storage stability, prevents phase separation, and maintains uniform dispersion and structural integrity in sol-gel-derived materials. Time-dependent strain-sweep (thixotropic) tests were conducted on the G10 organogel as well as its metallogels containing alkali metal ions: **G10-Li**, **G10-Na**, and **G10-K** (**Figure 4.15**). A cyclic strain starting with a low value of 1% was applied, where the storage modulus (G') was higher than the loss modulus (G''). Over time, the strain was gradually increased to 100%, which resulted in enhanced flow behavior of the gels, as shown by the loss modulus (G'') exceeding the storage modulus (G'). These tests were conducted over

five cycles, demonstrating the gel's ability to transition between sol and gel states.

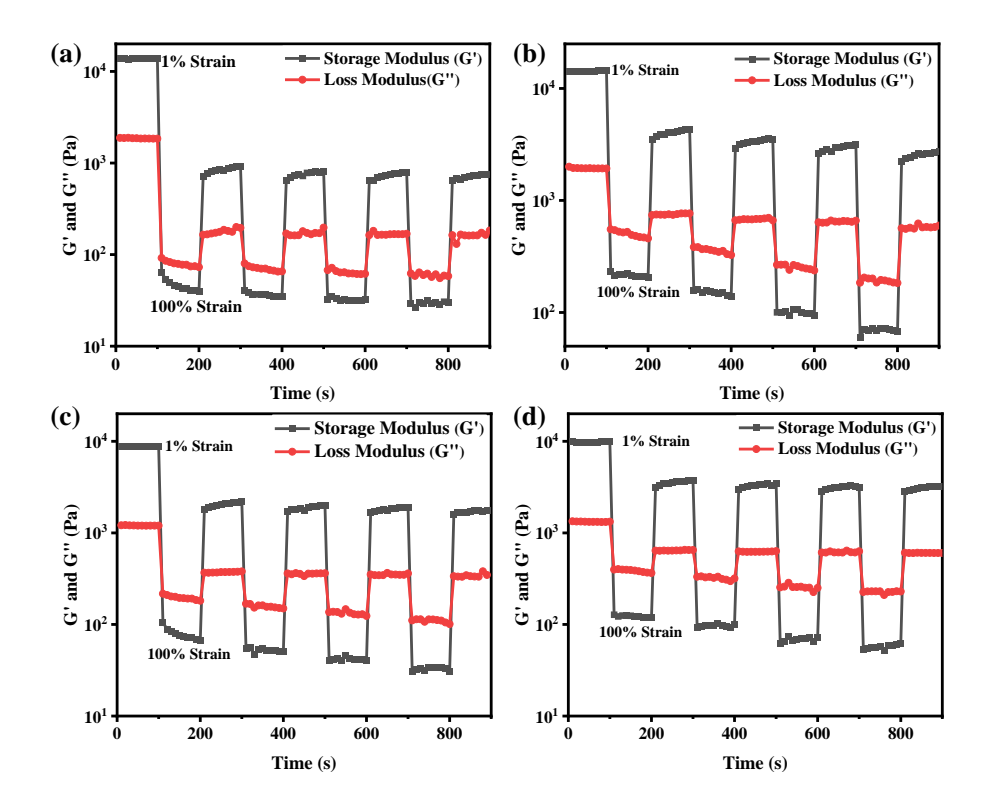
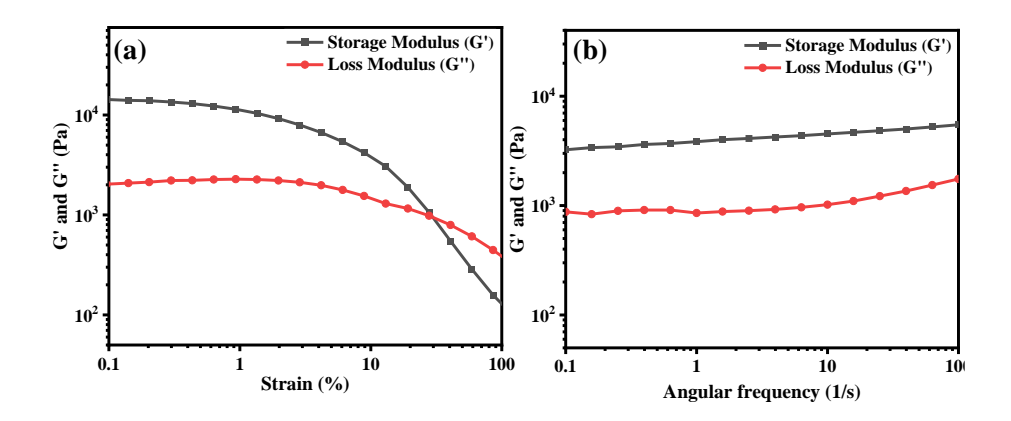


Figure 4.15: Strain sweep (thixotropic) experiments of (a) G10 organogel, (b) G10-Li metallogel, (c) G10-Na metallogel, and (d) G10-K metallogel

# 4.8.2 G10-Dox organogel

The average storage modulus (G') of the **G10-Dox** organogel was 1.40 × 10<sup>4</sup> Pa, where the storage modulus (G') was greater than the loss modulus (G") initially. Upon increasing the strain, the linearity of G' and G" deviated, and a crossover point was observed at approximately 28% of strain, above which the loss modulus was greater than the storage modulus. The angular frequency-sweep experiments of **G10-Dox** organogel were carried out to confirm the viscoelastic properties of the gel (**Figure 4.16**).



**Figure 4.16:** (a) Linear viscoelastic (LVE) range and angular frequency sweep (b) of **G10-Dox** organogel

Thixotropy is particularly important in drug delivery as it allows formulations to have low viscosity under shear, facilitating easy injection, spreading, or application, while quickly returning to a semisolid or gel-like state after administration. A time-dependent strainsweep (thixotropic) test was performed on the **G10-Dox** organogel. A cyclic strain, starting at a low 1%, was applied, where the storage modulus (G') exceeded the loss modulus (G"). Over time, the strain was gradually increased to 100%, which resulted in enhanced flow behavior of the gel, indicated by the loss modulus (G") surpassing the storage modulus (G'). This test was conducted for five cycles, demonstrating the gel's ability to transition between sol and gel states (**Figure 4.17**).

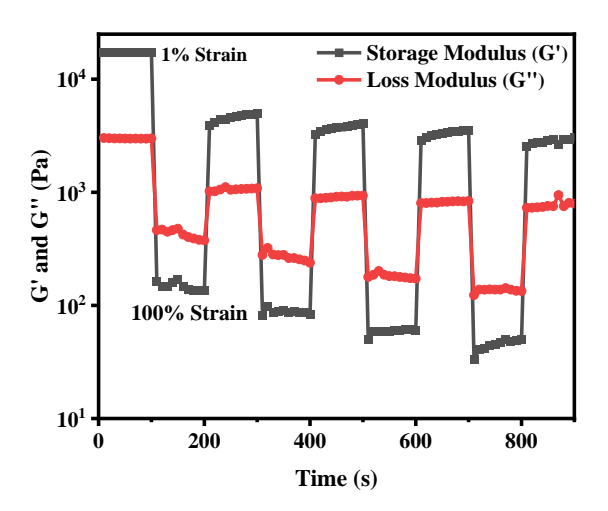


Figure 4.17: Strain-sweep (thixotropic) experiment of G10-Dox organogel

#### 4.9 PXRD Analysis

The interactions between the gelator molecule **G10** and **G10** xerogel were analyzed using the PXRD technique (**Figure 4.18**). The gelator molecule **G10** exhibits peaks at  $2\theta = 15.24^{\circ}$  (d = 5.79A°) for intercolumnar stacking, and peaks at  $2\theta = 21.43^{\circ}$  (d = 4.14A°),  $2\theta = 24.37^{\circ}$  (d = 3.65A°),  $2\theta = 25.11^{\circ}$  (d = 3.55A°),  $2\theta = 26.20^{\circ}$  (d = 3.39A°),  $2\theta = 26.94^{\circ}$  (d = 3.31A°),  $2\theta = 27.88^{\circ}$  (d = 3.19A°) for  $\pi$ - $\pi$  stacking. Upon the analysis of the spectra of **G10** xerogel, a peak at  $2\theta = 16.61^{\circ}$  (d = 5.35A°) for inter-columnar stacking and peaks at  $2\theta = 22.33^{\circ}$  (d = 3.97A°),  $2\theta = 27.20^{\circ}$  (d = 3.28A°) for  $\pi$ - $\pi$  stacking were observed.<sup>35</sup> Compared to **G10** powder, a few broader peaks were observed in **G10** xerogel due to the less crystallinity or amorphous nature of xerogel.

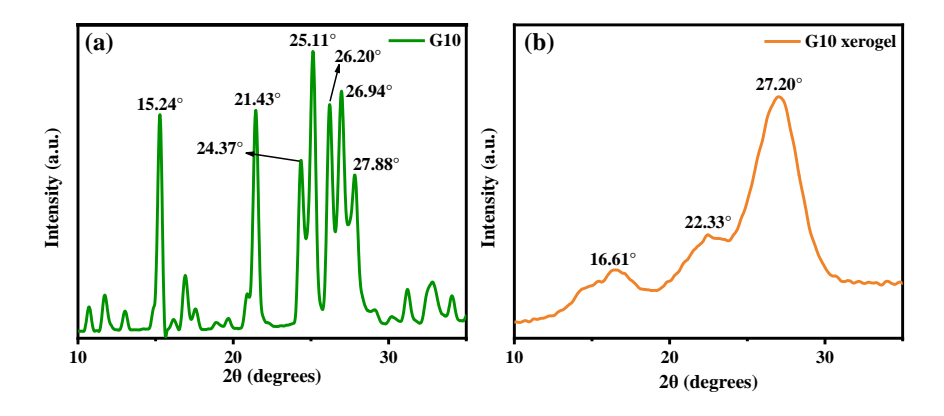


Figure 4.18: PXRD spectra of (a) gelator G10 and (b) G10 xerogel

Further, the PXRD analysis of **G10-Dox** xerogel (**Figure 4.19**) showed similar broad peaks at 16.02°, 23.05°, and 26.94°, °similar to that of **G10** xerogel. This is due to the gel's low crystalline and amorphous nature induced by the non-covalent interactions.

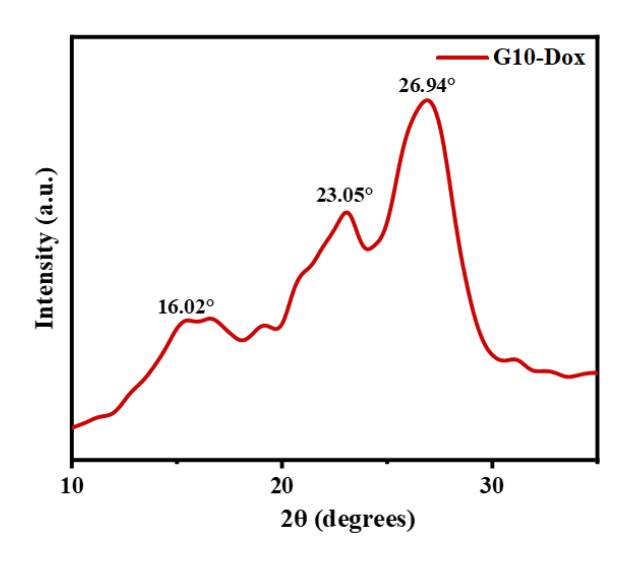


Figure 4.19: PXRD spectrum of G10-Dox xerogel

# 4.10 Thermogravimetric Analysis

The thermal stability of the gelator molecule G10 and xerogels of G10 and G10-Dox organogel were examined using thermogravimetric analysis within the temperature range of 30-800°C.

# 4.10.1 The gelator molecule G10

The gelator molecule showed a weight loss of 11% up to 167 °C, possibly due to the loss of entrapped solvents on the molecule's surface. Further, between 167-306°C, a weight loss of 20% was observed due to the decarboxylation of the two -COOH groups and the thermally labile -CH=N- linkage breakdown (Figure 4.20).

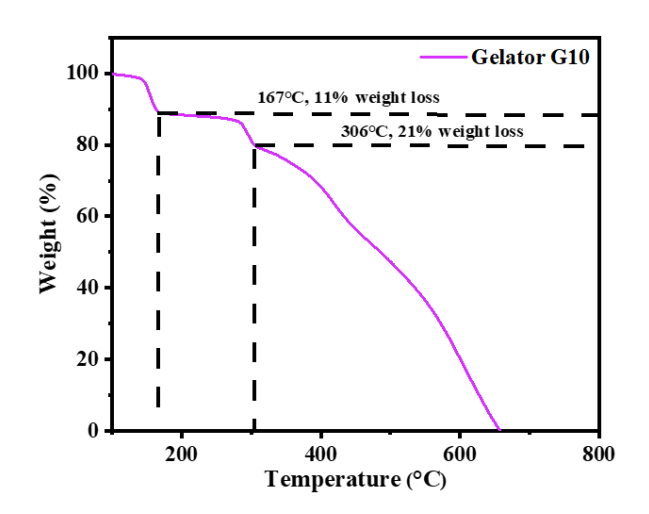


Figure 4.20: TGA analysis of gelator molecule G10

#### 4.10.2 G10 and G10-Dox organogel

For G10 and G10-Dox organogel, a minimal weight loss of 12% was observed at 217°C and 193°C, respectively, which is possibly due to the breakdown of the non-covalent interactions that aided in the formation of the gel. In the case of G10 xerogel, complete combustion without a residue is observed at 670°C. Still, in G10-Dox xerogel, about 25% of the residue remains at the same temperature, which might be due to the stable Dox-gelator complexes (Figure 4.21).

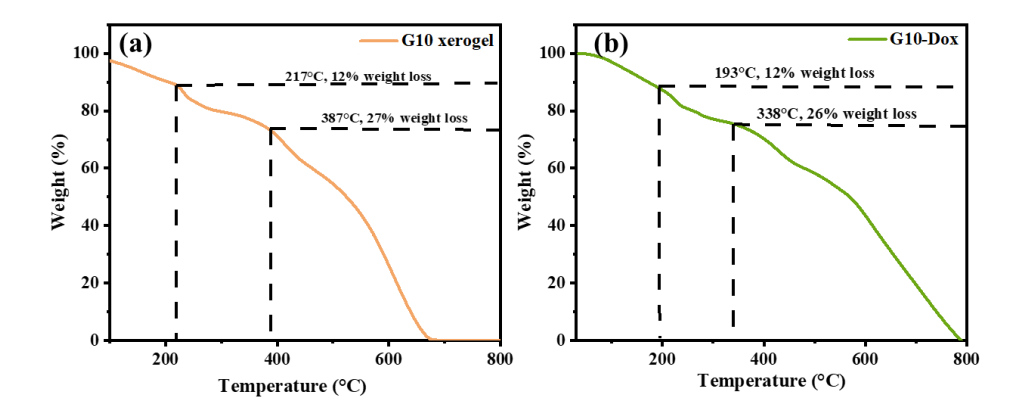


Figure 4.21: TGA analysis of (a) G10 and (b)G10-Dox xerogel

# 4.11 FE-SEM Analysis

The morphology of the gelator molecule and the xerogels was analysed using FE-SEM. Gelator molecule G10 shows a spherical type morphology (Figure 4.22). Upon examining the morphology of the xerogel of organogels and metallogels fabricated from the molecule, notable changes were noted. The morphology of xerogels of G10, G10-Na, and G10-K was of dense fibrillar network structure (Figure 4.23). This change was due to the self-organization of the gelator molecules that formed the gel.

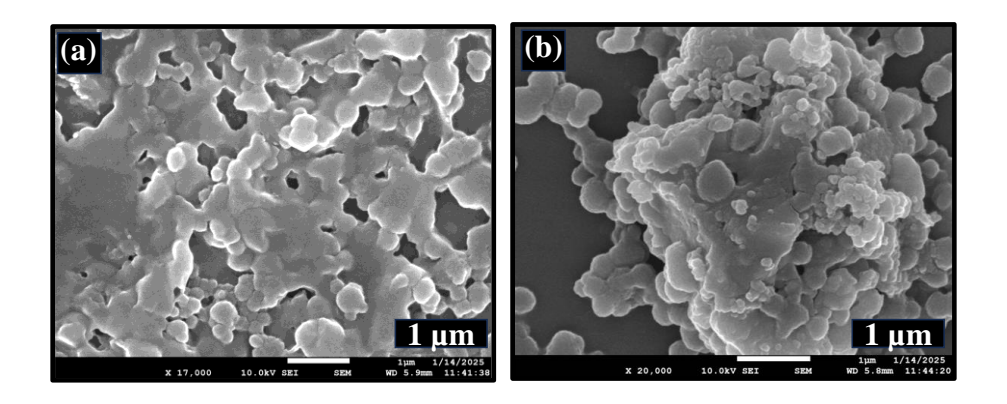


Figure 4.22: FE-SEM image of gelator molecule G10

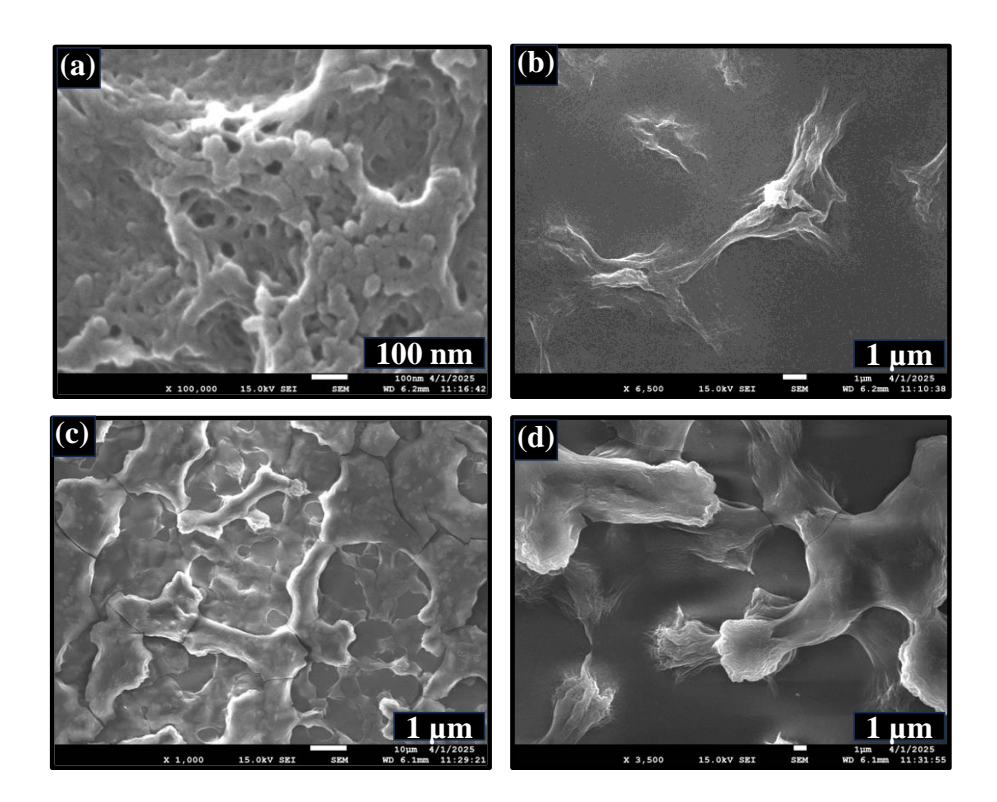


Figure 4.23: FE-SEM images of (a), (b) G10 xerogel, (c) G10-Na xerogel, and (d) G10-K xerogel

Similarly, dense fibrillar networks were also observed for **G10-Dox** xerogel (Figure 4.24).

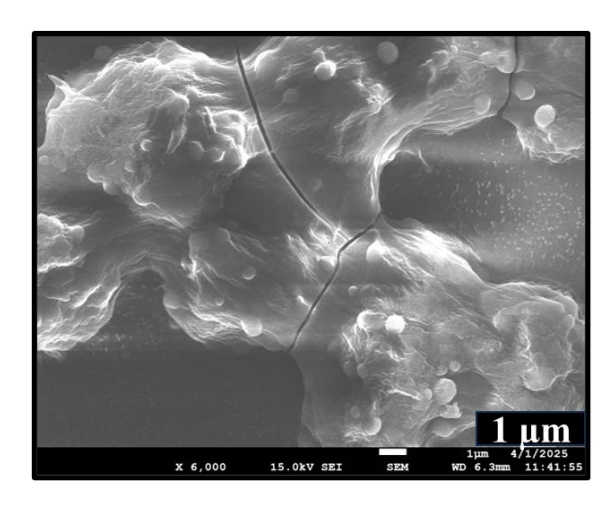


Figure 4.24: FE-SEM image of G10-Dox xerogel

The morphological transformation from the spherical gelator molecules to a dense fibrillar network in the xerogels is evidence of the selforganization of molecules by various molecular interactions.

# 4.12 Self-healing and injectability of G10-Dox organogel

Injectability allows for minimally invasive administration, enabling the gel to be delivered precisely to irregular or hard-to-reach target sites. Once administered, self-healing ensures that the gel can restore its structure after injection-induced shear or deformation, maintaining its integrity as a drug reservoir. This helps achieve sustained and localized drug release, enhances retention at the target site, and improves therapeutic efficacy, all while reducing systemic side effects. The self-healing properties of the **G10-Dox** organogel were tested by cutting the center of the gel. After standing for 10 minutes, the material began to self-repair without the need for any external stimuli, and the cut was sealed (**Figure 4.25**).

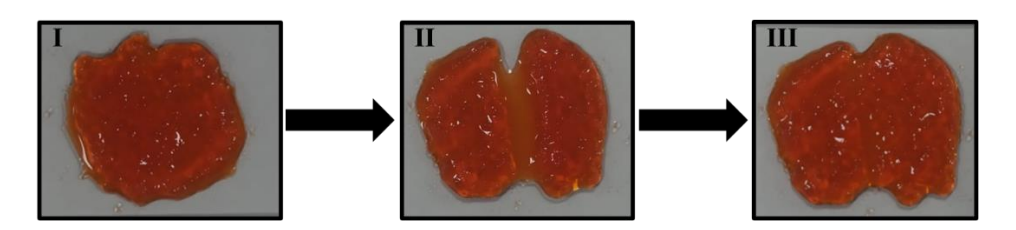


Figure 4.25: Images showing the self-healing property of G10-Dox organogel

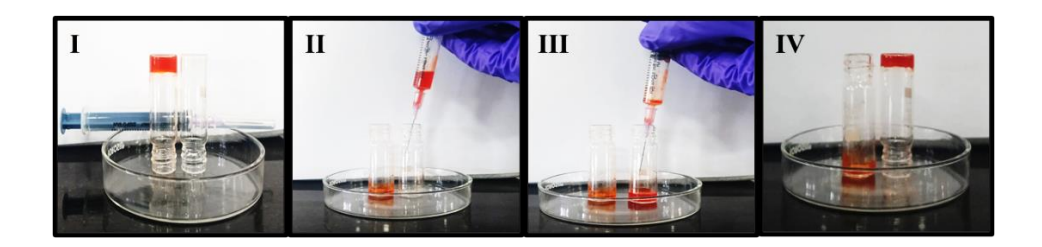


Figure 4.26: Images showing the injectability of G10-Dox organogel

# 4.13 UV-Vis Spectra Analysis

The UV-Vis spectra of **G10** organogel were recorded in solution state in a 1:1 DMSO: H<sub>2</sub>O mixture. Upon analysis, a sharp peak was observed at 286 nm and a broad one at 337 nm (**Figure 4.27**). These peaks are presumably associated with  $\pi$ - $\pi$ \* transitions of aromatic moieties and n- $\pi$ \* transitions of the Schiff base moiety, respectively.

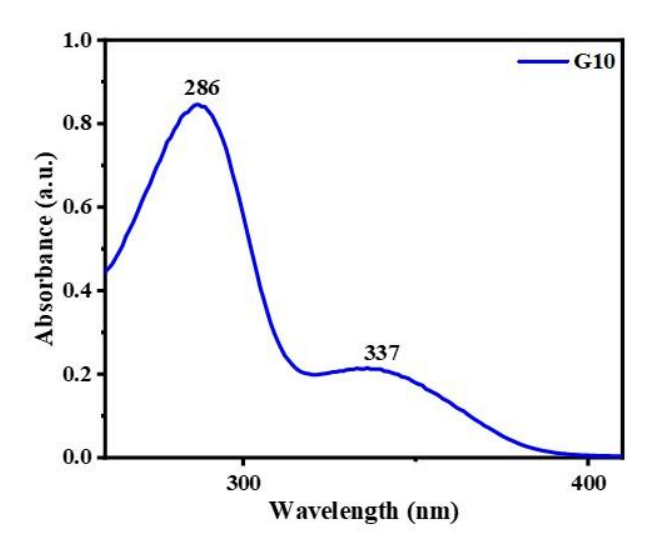


Figure 4.27: UV-Visible spectrum of G10

# 4.14 Fluorescence Spectra analysis

The fluorescence emission spectra of **G10** were recorded in a DMSO: H<sub>2</sub>O mixture by exciting the molecule at a wavelength of 330 nm. A highly intense peak was observed in the emission spectra at 430 nm (**Figure 4.28**).

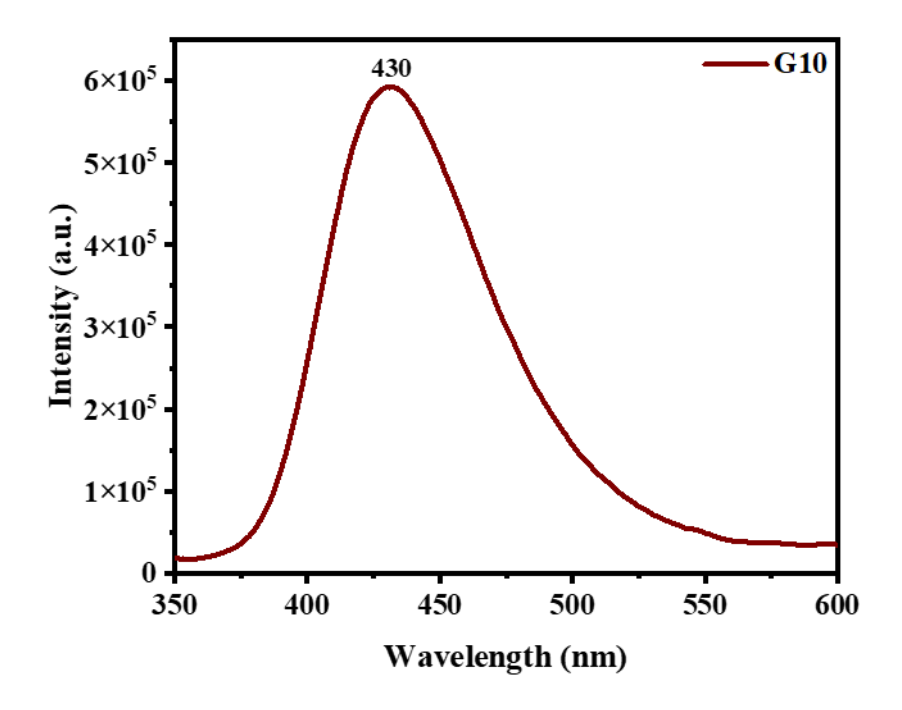
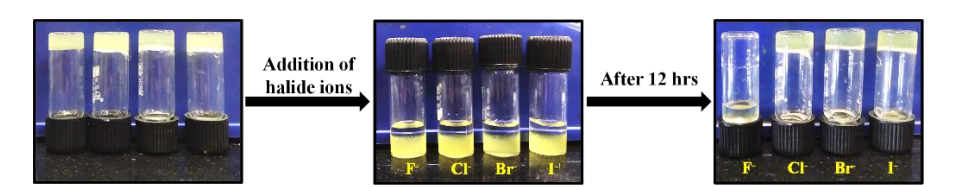


Figure 4.28: Fluorescence spectrum of G10

#### 4.15 Visual and Fluorometric detection with fluoride ions

1 mL of **G10** organogel was tplaced in 4 separate glass vials, and 1 mL of a 1 mM solution of halide ions F-, Cl-, Br-, and I- was added on top of the gel. It was observed that F<sup>-</sup> ion can induce gel-to-sol transition in 12 hours (**Figure 4.29**).



**Figure 4.29:** Images showing the gel-to-sol transition of **G10** organogel after the addition of fluoride ions.

Further, the fluorescence spectra of **G10** were analysed after the addition of halide ions, and it was found that the  $F^-$  ion caused changes in the spectrum of **G10** (**Figure 4.30**). A decreased intensity and slight blue shift towards 42 nm were observed in the emission spectra of **G10** upon the addition of fluoride ions. This might be due to the interaction of the  $F^-$  ion with the imidazolic N-H group, which disrupts the  $\pi$ -conjugation.

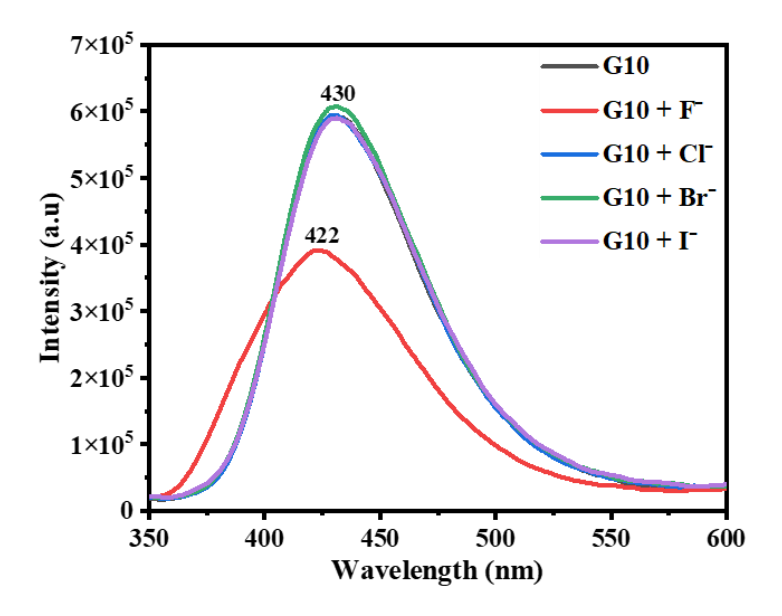


**Figure 4.30:** Changes in the emission spectra of **G10** upon the addition of halide ions

# 4.16 Cell viability assay

The cytotoxicity of imidazole and G10 was assessed using the MTT assay. HEK293 cells were seeded at a density of 10,000 cells per well in a 96-well plate and treated with varying concentrations of imidazole and G10. After 24 hours, the media was removed, and 0.5 mg/mL MTT reagent was added to each well. The cells were then incubated for 3 hours at 37°C in the dark. Following incubation, DMSO was added to dissolve the formazan crystals, and the plate was shaken on an orbital shaker at 220 rpm for 2 hours at room temperature. Cell viability was determined by measuring the absorbance at 500 nm..

The compound **G10** showed good biocompatibility with an IC<sub>50</sub> value of 390.6  $\mu$ M (Figure 4.31).

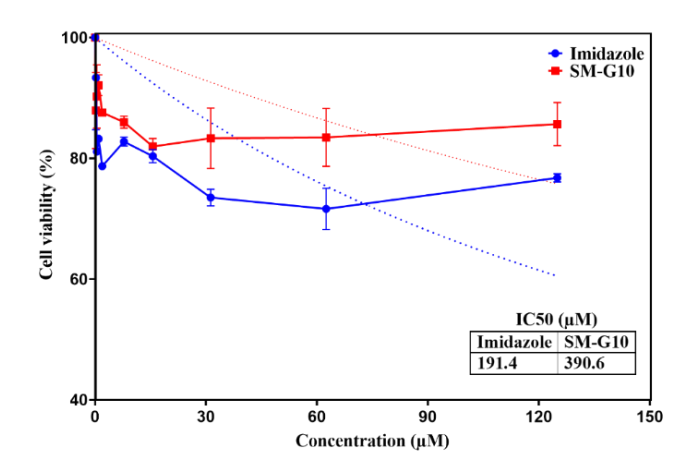


**Figure 4.31:** Determination of cytotoxicity through MTT assay of **G10** in HEK293 cell line

# 4.17 Encapsulation efficiency and drug release study

Gels have been successfully utilized as drug delivery vehicles because of their swelling and diffusion of the cargo material inside them into the surrounding medium when immersed in a solution in a controlled manner.<sup>36</sup> The **G10-Dox** organogel was formed by the in situ encapsulation of the drug, which controls the concentration and even distribution of drug molecules inside the gel.

The gel was washed with 3 mL PBS buffer to remove the unbound drug molecules, and the absorbance of the supernatant was measured using a UV-Visible spectrometer. As doxorubicin exhibits an absorbance peak at 480 nm, the absorbance of the initial concentration and the concentration of the supernatant solution were analysed. Different concentration solution of doxorubicin was analysed using UV-Vis spectroscopy to calculate the amount of drug released at a specific absorbance value, and a calibration curve was plotted (Figure 4.32). The amount of drug encapsulated was calculated by subtracting the drug present in the supernatant from the initial amount using the calibration curve drawn by varying the concentration of doxorubicin (Figure 4.33).

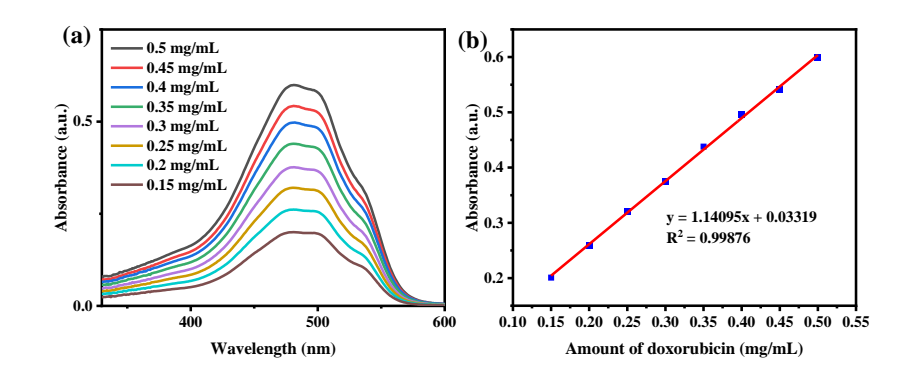


**Figure 4.32: (a)** UV-Vis spectra of different concentration solutions of doxorubicin in PBS buffer and **(b)** Calibration curve

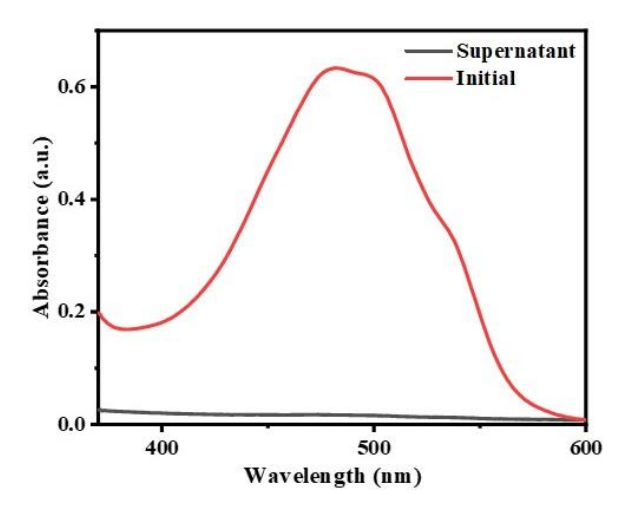


**Figure 4.33:** Evaluation of encapsulation efficiency of doxorubicin from UV-Vis spectroscopy

UV absorbance at 480 nm (Initial) = 0.6310

UV absorbance at 480 nm (supernatant after washing) = 0.0175

From the calibration curve, y = 1.14095x + 0.03319,  $R^2 = 0.99876$  where y = absorbance, x = concentration of doxorubicin (mg mL<sup>-1</sup>)

Concentration (Calculation from the curve)

Initial concentration (C<sub>1</sub>): 0.52395 mg mL<sup>-1</sup>

The concentration of unloaded drug in the supernatant ( $C_2$ ): 0.01453 mg  $mL^{-1}$ 

Encapsulation efficiency =  $\frac{C_1 - C_2}{C_1} \times 100 = 97\%$ 

The encapsulation efficiency was found to be 97%.

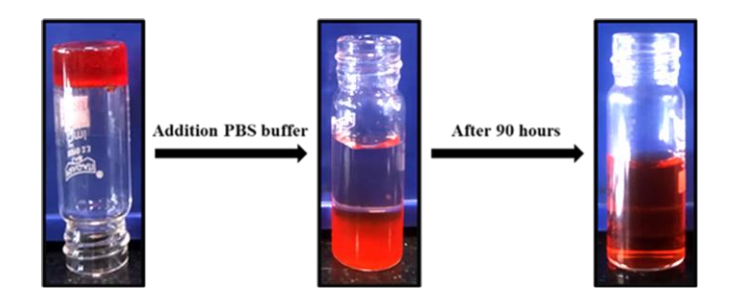


**Figure 4.34:** Images showing the drug delivery of doxorubicin after the addition of PBS buffer to **G10-Dox** organogel

The sustained drug release from the organogel was studied by adding 3 mL of PBS buffer on top of 1 mL of the gel in a glass vial. The complete collapse of the gel and further release of the drug were observed after 90 hours (**Figure 4.32**). The drug release was monitored by collecting 400  $\mu$ L of the supernatant solution from the vial, which was replaced by fresh PBS solution at a specific time interval. The absorbance of the collected sample was measured at a wavelength of 480 nm, which is the absorbance peak of doxorubicin, using UV-Visible spectrometry.

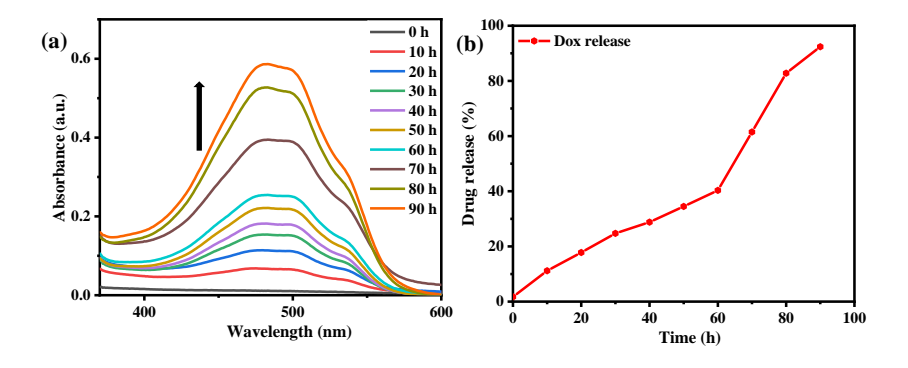


**Figure 4.35:** (a) UV-Visible spectra and (b) release profile of time-dependent drug release from **G10-Dox** organogel at pH 7.4

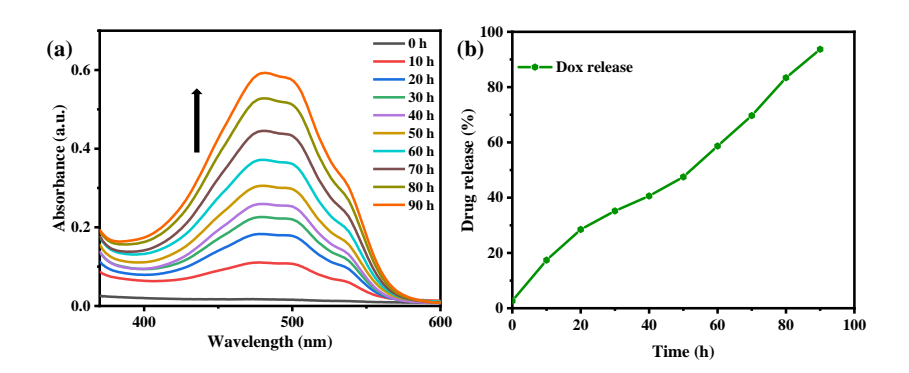


**Figure 4.36:** (a) UV-Visible spectra and (b) release profile of time-dependent drug release from **G10-Dox** organogel at pH 4.8

The time-dependent release of doxorubicin drug from **G10-Dox** organogel was studied at a neutral pH of 7.4 (**Figure 4.33**) and an acidic pH of 4.8 (**Figure 4.34**). It was observed that 92% and 94% of the drug was released at pH 7.4 and 4.8, respectively, after 90 hours.

# CHAPTER 5

#### **CONCLUSION AND FUTURE SCOPE**

#### 5.1 Conclusion

he low molecular weight Schiff base gelator G10 was synthesized through an efficient one-step reaction from readily available precursors and well characterized by mass spectrometry, NMR, and FTIR spectroscopy. The resultant organogels based on G10 exhibited significant stimuli-responsive properties, especially towards transition metal and fluoride ions. Fluoride detection was assessed visually through gel-to-sol transitions as well as fluorometrically through monitoring a shift and decrease in emission peak intensity.

Moreover, metallogels containing alkali metal ions were developed successfully. Rheological measurements established the mechanical stability and thixotropy of the gels. Cytotoxicity tests showed that G10 is biocompatible, demonstrating its scope for biomedical applications. Furthermore, an injectable and self-healing organogel, G10-Dox, was prepared by loading doxorubicin. The gel released the drug over 90 hours continuously, with 94% drug release in a controlled fashion.

#### **5.2** Future scope

This research has explored the release of the drug from the G10 organogel in pH-buffered conditions. Further, there is a need to explore the drug delivery from the gel matrix in the presence of other external stimuli. The cell viability of the cancerous cell line in the presence of the G10-Dox organogel also needs to be explored.

#### **REFERENCES**

- (1) Dastidar, P. Supramolecular Gelling Agents: Can They Be Designed? *Chem. Soc. Rev.* **2008**, *37* (12), 2699. https://doi.org/10.1039/b807346e.
- (2) Rogovina, L. Z.; Vasil'ev, V. G.; Braudo, E. E. Definition of the Concept of Polymer Gel. *Polym. Sci. Ser. C* **2008**, *50* (1), 85–92. https://doi.org/10.1134/S1811238208010050.
- (3) Amabilino, D. B.; Smith, D. K.; Steed, J. W. Supramolecular Materials. *Chem. Soc. Rev.* **2017**, *46* (9), 2404–2420. https://doi.org/10.1039/C7CS00163K.
- (4) Estroff, L. A.; Hamilton, A. D. Water Gelation by Small Organic Molecules. *Chem. Rev.* **2004**, *104* (3), 1201–1218. https://doi.org/10.1021/cr0302049.
- (5) Pham, Q. N.; Brosse, N.; Frochot, C.; Dumas, D.; Hocquet, A.; Jamart-Grégoire, B. Influence of the Gelator Structure and Solvent on the Organisation and Chirality of Self-Assembling Fibrillar Networks. *New J. Chem.* **2008**, *32* (7), 1131. https://doi.org/10.1039/b714375c.
- (6) Ahn, S.; Kasi, R. M.; Kim, S.-C.; Sharma, N.; Zhou, Y. Stimuli-Responsive Polymer Gels. *Soft Matter* **2008**, *4* (6), 1151. https://doi.org/10.1039/b714376a.
- (7) Panja, S.; Adams, D. J. Stimuli Responsive Dynamic Transformations in Supramolecular Gels. *Chem. Soc. Rev.* **2021**, *50* (8), 5165–5200. https://doi.org/10.1039/D0CS01166E.
- (8) Chen, L.; Raeburn, J.; Sutton, S.; Spiller, D. G.; Williams, J.; Sharp, J. S.; Griffiths, P. C.; Heenan, R. K.; King, S. M.; Paul, A.; Furzeland, S.; Atkins, D.; Adams, D. J. Tuneable Mechanical Properties in Low Molecular Weight Gels. *Soft Matter* **2011**, *7* (20), 9721. https://doi.org/10.1039/c1sm05827d.
- (9) Sangeetha, N. M.; Maitra, U. Supramolecular Gels: Functions and Uses. *Chem. Soc. Rev.* **2005**, *34* (10), 821. https://doi.org/10.1039/b417081b.
- (10) Yamauchi, A. GelsIntroduction. In *Gels Handbook*; Elsevier, 2001; Vol. 1, pp 4–12. https://doi.org/10.1016/B978-012394690-4/50075-X.

- (11) Terech, P.; Weiss, R. G. Low Molecular Mass Gelators of Organic Liquids and the Properties of Their Gels. *Chem. Rev.* **1997**, 97 (8), 3133–3160. https://doi.org/10.1021/cr9700282.
- (12) Chu, C.-W.; Schalley, C. A. Recent Advances on Supramolecular Gels: From Stimuli-Responsive Gels to Co-Assembled and Self-Sorted Systems. *Org. Mater.* **2021**, *03* (01), 025–040. https://doi.org/10.1055/s-0040-1722263.
- (13) Sakai, T.; Katashima, T.; Matsushita, T.; Chung, U. Sol-Gel Transition Behavior near Critical Concentration and Connectivity. *Polym. J.* **2016**, *48* (5), 629–634. https://doi.org/10.1038/pj.2015.124.
- (14) Shapiro, Y. E. Structure and Dynamics of Hydrogels and Organogels: An NMR Spectroscopy Approach. *Prog. Polym. Sci.* **2011**, 36 (9), 1184–1253. https://doi.org/10.1016/j.progpolymsci.2011.04.002.
- Yang, M.; Zhang, Z.; Yuan, F.; Wang, W.; Hess, S.; Lienkamp, K.; Lieberwirth, I.; Wegner, G. Self-Assembled Structures in Organogels of Amphiphilic Diblock Codendrimers. *Chem. Eur. J.* 2008, 14 (11), 3330–3337. https://doi.org/10.1002/chem.200701731.
- (16) Li, S.-L.; Xiao, T.; Hu, B.; Zhang, Y.; Zhao, F.; Ji, Y.; Yu, Y.; Lin, C.; Wang, L. Formation of Polypseudorotaxane Networks by Cross-Linking the Quadruple Hydrogen Bonded Linear Supramolecular Polymers via Bisparaquat Molecules. *Chem. Commun.* **2011**, *47* (38), 10755. https://doi.org/10.1039/c1cc14559b.
- (17) Yan, C.; Pochan, D. J. Rheological Properties of Peptide-Based Hydrogels for Biomedical and Other Applications. *Chem. Soc. Rev.* **2010**, *39* (9), 3528. https://doi.org/10.1039/b919449p.
- (18) Pasparakis, G.; Vamvakaki, M. Multiresponsive Polymers: Nano-Sized Assemblies, Stimuli-Sensitive Gels and Smart Surfaces. *Polym. Chem.* **2011**, *2* (6), 1234. https://doi.org/10.1039/c0py00424c.
- (19) Kamaly, N.; Yameen, B.; Wu, J.; Farokhzad, O. C. Degradable Controlled-Release Polymers and Polymeric Nanoparticles: Mechanisms of Controlling Drug Release. *Chem. Rev.* **2016**, *116* (4), 2602–2663. https://doi.org/10.1021/acs.chemrev.5b00346.

- (20) Webber, M. J.; Langer, R. Drug Delivery by Supramolecular Design. *Chem. Soc. Rev.* **2017**, *46* (21), 6600–6620. https://doi.org/10.1039/C7CS00391A.
- (21) Yang, X.; Zhang, G.; Zhang, D. Stimuli Responsive Gels Based on Low Molecular Weight Gelators. *J Mater Chem* **2012**, *22* (1), 38–50. https://doi.org/10.1039/C1JM13205A.
- (22) Adams, D. J.; Morris, K.; Chen, L.; Serpell, L. C.; Bacsa, J.; Day, G. M. The Delicate Balance between Gelation and Crystallisation: Structural and Computational Investigations. *Soft Matter* **2010**, *6* (17), 4144. https://doi.org/10.1039/c0sm00409j.
- (23) Mukherjee, S.; Paul, A. K.; Stoeckli-Evans, H. A Family of Highly Selective Fluorescent Sensors for Fluoride Based on Excited State Proton Transfer Mechanism. *Sens. Actuators B Chem.* **2014**, *202*, 1190–1199. https://doi.org/10.1016/j.snb.2014.06.034.
- (24) Panja, A.; Ghosh, K. Azo and Imine Functionalized 2-Naphthols: Promising Supramolecular Gelators for Selective Detection of Fe<sup>3+</sup> and Cu<sup>2+</sup>, Reactive Oxygen Species and Halides. *Mater. Chem. Front.* **2018**, *2* (10), 1866–1875. https://doi.org/10.1039/C8QM00257F.
- (25) Wang, Y.; Xiong, J.; Peng, F.; Li, Q.; Zeng, M.-H. Building a Supramolecular Gel with an Ultra-Low-Molecular-Weight Schiff Base Gelator and Its Multiple-Stimulus Responsive Properties. *Colloids Surf. Physicochem. Eng. Asp.* **2022**, *640*, 128445. https://doi.org/10.1016/j.colsurfa.2022.128445.
- (26) Tseng, Y.-C.; Xu, Z.; Guley, K.; Yuan, H.; Huang, L. Lipid–Calcium Phosphate Nanoparticles for Delivery to the Lymphatic System and SPECT/CT Imaging of Lymph Node Metastases. *Biomaterials* **2014**, *35* (16), 4688–4698. https://doi.org/10.1016/j.biomaterials.2014.02.030.
- (27) Li, Y.; Maciel, D.; Rodrigues, J.; Shi, X.; Tomás, H. Biodegradable Polymer Nanogels for Drug/Nucleic Acid Delivery. *Chem. Rev.* 2015, 115 (16), 8564–8608. https://doi.org/10.1021/cr500131f.
- (28) Sun, W.; Gu, Z. Engineering DNA Scaffolds for Delivery of Anticancer Therapeutics. *Biomater. Sci.* **2015**, *3* (7), 1018–1024. https://doi.org/10.1039/C4BM00459K.

- (29) Thakur, N.; Sharma, B.; Bishnoi, S.; Jain, S.; Nayak, D.; Sarma, T. K. Biocompatible Fe<sup>3+</sup> and Ca<sup>2+</sup> Dual Cross-Linked G-Quadruplex Hydrogels as Effective Drug Delivery System for pH-Responsive Sustained Zero-Order Release of Doxorubicin. *ACS Appl. Bio Mater.* **2019**, *2* (8), 3300–3311. https://doi.org/10.1021/acsabm.9b00334.
- (30) Zare, D.; Yılmaz, G.; Özçubukçu, S. Application of Redox-Responsive Cysteine-Based Organogels as a Drug Delivery System for Doxorubicin. *ACS Omega* **2025**, *10* (1), 147–156. https://doi.org/10.1021/acsomega.4c02620.
- (31) Ritik; Sarkar, S.; Pragti; Varshney, N.; Kumar, A.; Kuznetsov, M. L.; Jha, H. C.; Mukhopadhyay, S. Nano-Structured Gel Materials for Environmental Remediation and Biomedical Applications. *ACS Appl. Nano Mater.* **2024**, *7* (18), 22292–22303. https://doi.org/10.1021/acsanm.4c04684.
- (32) Boiani, M.; Gonzalez, M. Imidazole and Benzimidazole Derivatives as Chemotherapeutic Agents. *Mini-Rev. Med. Chem.* **2005**, *5* (4), 409–424. https://doi.org/10.2174/1389557053544047.
- (33) Calu, L.; Badea, M.; Chifiriuc, M. C.; Bleotu, C.; David, G.-I.; Ioniță, G.; Măruțescu, L.; Lazăr, V.; Stanică, N.; Soponaru, I.; Marinescu, D.; Olar, R. Synthesis, Spectral, Thermal, Magnetic and Biological Characterization of Co(II), Ni(II), Cu(II) and Zn(II) Complexes with a Schiff Base Bearing a 1,2,4-Triazole Pharmacophore. *J. Therm. Anal. Calorim.* **2015**, *120* (1), 375–386. https://doi.org/10.1007/s10973-014-3970-5.
- (34) Wang, X.; Cui, W.; Li, B.; Zhang, X.; Zhang, Y.; Huang, Y. Supramolecular Self-Assembly of Two-Component Systems Comprising Aromatic Amides/Schiff Base and Tartaric Acid. *Front. Chem. Sci. Eng.* **2020**, *14* (6), 1112–1121. https://doi.org/10.1007/s11705-019-1865-5.
- (35) Zhang, Z.; Zhang, S.; Zhang, J.; Zhu, L.; Qu, D. Solvent-Dependent Self-Assembly and Morphological Transition of Low-Molecular-Weight Azobenzene Organogel. *Tetrahedron* **2017**, *73* (33), 4891–4895. https://doi.org/10.1016/j.tet.2017.05.027.
- (36) Radin, S.; Chen, T.; Ducheyne, P. The Controlled Release of Drugs from Emulsified, Sol Gel Processed Silica Microspheres. *Biomaterials* **2009**, *30* (5), 850–858. https://doi.org/10.1016/j.biomaterials.2008.09.066.